BET inhibition induces an anti-apoptotic adaptive response and therapeutic vulnerability to MCL1 inhibitors in breast cancer

Gonghong Yan[1], Heping Wang[1], Augustin Luna[2], Behnaz Bozorgui[1], Xubin Li[1], Zeynep Dereli[3], Xiaohua Chen[1], Yiling Lu[4], Ozgun Babur[5], Chis Sander[2,7], Gordon Mills[8,9], Anil Korkut[1,*]

[1] Department of Bioinformatics and Computational Biology, UT MD Anderson Cancer Center, Houston, TX, 77030, USA
[2] cBio Center, Dana Farber Cancer Institute, Boston, MA, 02215, USA
[3] Department of Neurosurgery, Houston Methodist Research Institute, Houston, TX, 77030, USA
[4] Department of Systems Biology, UT MD Anderson Cancer Center, Houston, TX, 77030, USA
[5] Department of Molecular and Medical Genetics, Oregon Health and Science University, Portland, OR, 97201, USA
[6] Computational Biology Program, Oregon Health and Science University, Portland, OR 97239, USA
[7] Department of Cell Biology, Harvard Medical School, Boston, MA, USA
[8] Department of Cell, Development and Cancer Biology, Oregon Health and Sciences University, Portland, OR 97201, USA
[9] Knight Cancer Institute, Oregon Health and Science University, Portland, OR, 97201, USA
*akorkut@mdanderson.org

Abstract

We have demonstrated that adaptive responses to BET inhibitors induce a therapeutic vulnerability to the combination of BET and MCL1 inhibitors in breast cancer. Our generalizable strategy for identification of adaptive responses and therapeutic vulnerabilities integrates our novel network analysis method, termed Target Score, with genomics and mechanistic perturbation biology studies. In drug resistant cells, adaptive responses to BET inhibitors involve upregulation of fatty acid metabolism coupled to changes in membrane fluidity, cell adhesion and motility, EGFR/HER2 pathway activation, and subsequent accumulation of MCL1 that drives apoptosis evasion. The combined inhibition of MCL1 and BET proteins is highly synergistic in diverse breast cancer models. MCL1 inhibition was found to be most effective, either as a single agent or in combination in tumors with MCL1 chromosomal amplifications, a frequent driver aberration in breast cancer. In conclusion, we have discovered a mechanism of resistance to BET inhibition and an anti-resistance combination therapy that can increase the therapeutic benefit for a significant fraction of breast cancer patients.

Introduction.

Despite the success of targeted therapies in cancer treatment, response to mono-therapies has been transient due to the almost inevitable emergence of resistance. Blocking the routes that lead to the emergence of resistance with combination therapy is the most promising strategy to date (Holohan et al., 2013, Kim et al., 2018). However, discovery of effective combination therapies is a daunting task due to complexity of the molecular landscapes of drug response. A key mechanism of resistance is the adaptive activation of compensatory processes, e.g. feedback loops in the short-term or secondary oncogenic alterations in the long-term, in response to targeting driver oncogenic processes (Taylor and Schlaepfer, 2018). Systematic approaches are needed to identify adaptive responses, reveal drug-induced vulnerabilities, and enable the development of rational combination therapies.

Epigenetic targeting of gene expression is an emerging therapeutic option for diverse cancer types (Bennet and Licht, 2018). Specifically, the Bromodomain and Extra-Terminal (BET) proteins, including BRD2, BRD3 and BRD4, are promising targets (Loven et al., 2013). BET proteins link epigenetic states to lineage-specific gene expression through binding to acetylated

histones and regulating transcriptional initiation and elongation downstream of enhancer sites (Figure 1A). Preclinical efficacy of BET-inhibitors (BETis) has led to clinical trials in diverse cancer types including triple negative breast cancers (TNBC) (Alqahtani et al., 2019) (Figure 1B). Despite its highly variable and context-specific functions, reduction in cell cycle progression in response to BET inhibition has been proposed as an underlying mechanism of response in cancer cells (Doroshow et al., 2017). BETis also provide the opportunity for discovery of drug-induced vulnerabilities and effective drug combinations in cancer. This is evidenced by a shift in molecular and phenotypic plasticity in response to BETi, leading to the activation of the WNT pathway in adult acute myeloid leukemia (Rathert et al., 2015), induction of homologous recombination deficiency through CtIP, a DNA damage response protein, in ovarian cancer (Sun et al., 2018), and emergence of BRD4-dependent persistent cells with altered differentiation-states after MEK and PI3K/mTOR inhibition in TNBC (Risom et al., 2018). However, the molecular and phenotypic response landscape of BETi, which may inform on the discovery of effective drug combinations, have not been adequately explored particularly in solid tumors (Andrieu et al., 2016). We hypothesize that a systematic analysis of molecular and phenotypic adaptive responses to BET inhibition will deliver effective combination therapies in breast and other cancers.

The backbone of our strategy is based on exploiting the adaptive resistance concept whereby tumor ecosystems rapidly adapt to stress engendered by targeted therapies. Adaptive responses, in turn, induce therapeutic vulnerabilities that can be exploited with rational combination therapies. The strength and relevance of the adaptive resistance paradigm have been demonstrated in several studies involving discovery of rational combination therapies (Sun et al., 2017, Muranen et al., 2012, and Duncan et al., 2012). As adaptive responses occur through protein network rewiring, our key component is a novel computational algorithm, termed Target Score that capitalizes on the proteomic drug response data and network analysis of adaptive responses. Target Score algorithm (i) successfully quantifies and visualizes the collective adaptive resistance responses; (ii) nominates combination therapies, involving the agent that induces adaptive responses and a second agent that targets the vulnerability induced by the adaptive response. Target Score algorithm adds significant value to the conventional analysis pipeline that focuses on abundance changes in individual molecules. First, our method nominates functionally related multi-molecule modules of adaptive resistance with higher chance of functional relevance. Second, the method predicts multiple actionable targets in each module increasing the chances for successful validation and translation. Thanks to the network module-based analysis, the method reduces the number of false positives by eliminating signals from proteins with no functional partners. Target Score can operate even with single sample experiments where the sample is treated with a single agent and then profiled. The method scales to thousands of samples each treated with hundreds of individual (or combinations of) drugs in multiple doses and interrogated for hundreds to thousands of molecular entities across multiple time points.

Here, we use the Target Score method combined with genomic analysis and mechanistic perturbation biology studies to identify mechanisms of adaptive responses to BET inhibition. We discovered an anti-apoptotic adaptive response to BET inhibitors and a resultant therapeutic vulnerability, which is effectively targeted with a newly discovered combination of BET and MCL1 inhibitors.

Results

Breast cancer cells have differential responses to BET inhibition

To address the efficacy spectrum, predictors of response, and mechanisms of resistance to BET inhibition, we profiled cellular and proteomic responses to targeting BET in a series of breast

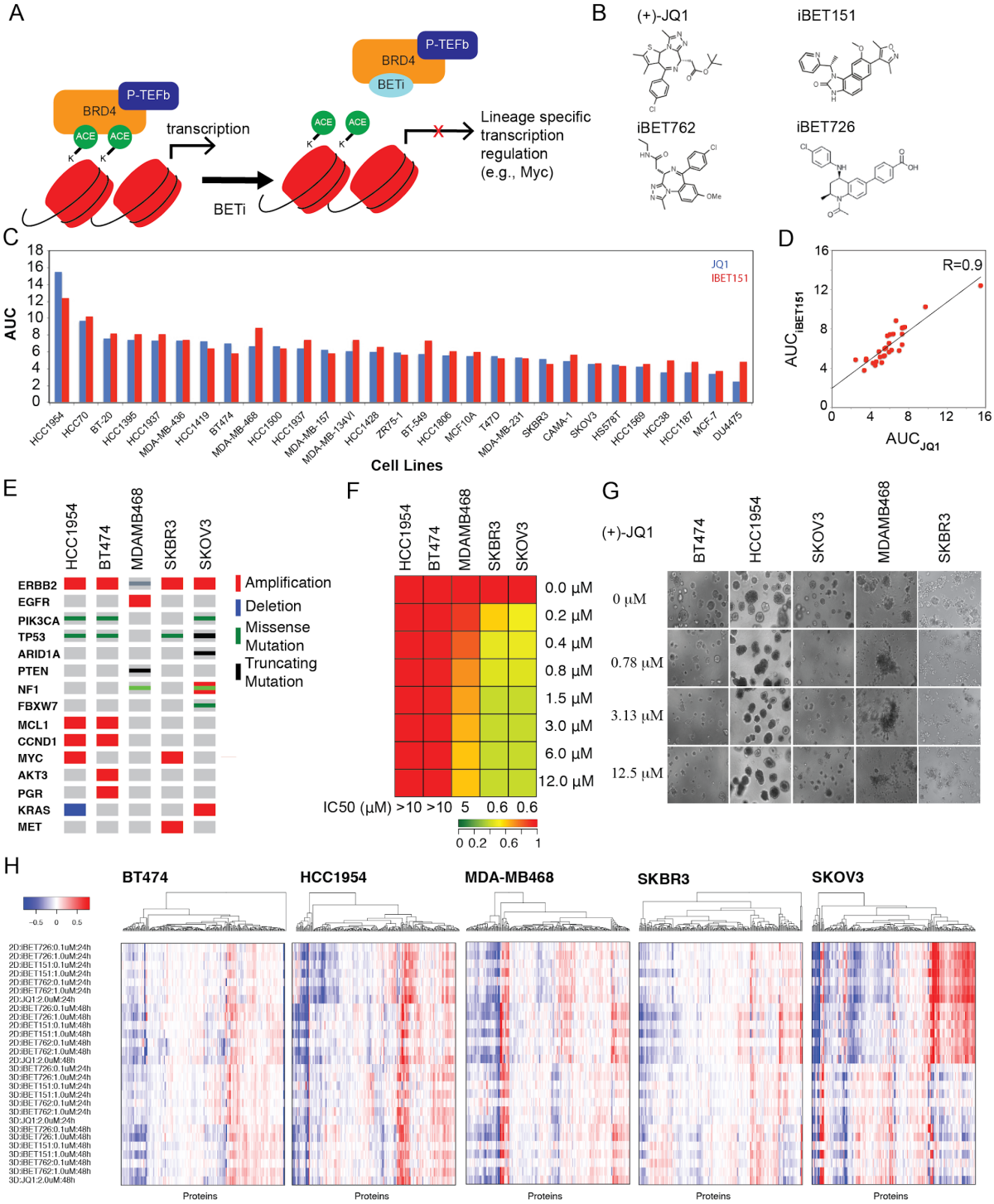

Figure 1. Response to BET inhibition in breast cancer. A. *BETis bind to acetyl histone binding cavity on BRD4 to prevent recruitment of BRD4 to chromatins and effect expression of lineage specific genes including but not limited to MYC.* ***B.*** *Chemical structures of BETis used in perturbation experiments.* ***C.*** *The relative responses to BETis JQ1 and iBET151 across 28 breast cancer lines and the ovarian line SKOV3 is quantified as area under the curve (AUC) of dose-response relationship (dose range 0-10 μM).* ***D.*** *The scatter plot of responses to IBET151 vs. JQ1 across the cell lines quantify the similarity in the phenotypic response to the two BETis.* ***E.*** *The landscape of potential driver oncogenic events in select breast and ovarian cancer cell lines.* ***F.*** *The dose-dependent response to JQ1 in the cell lines that are cultured in spherical matrigel medium.* ***G.*** *Dose-dependent viability responses to BETi in 3D cultures.* ***G.*** *Images of the*

dose-dependent responses to JQ1 in 3D matrigel cultured cells. ***H****. Proteomic response map of cell lines to BET inhibition. The proteomic data is collected with RPPA using antibodies that quantify levels of 218 total or phosphoprotein levels (2 time points, 2D and 3D cultures, varying doses of the four BETis).*

---

cancer cell lines. The cell viability responses to BET inhibition in 29 breast and ovarian cancer cell lines with varying genomic properties (Figure S1A) are quantified by the area under the curve (AUC) of dose-response relations (Figure 1C) and IC50 (Figure S1B) for JQ1 and IBET151. The comparison of JQ1 and IBET151 reveals a high correlation in cell viability response (R=0.91), suggesting that both compounds have similar efficacies and targets in vitro (Figure 1D). A correlative genomic analysis of response to BET inhibition did not detect a significant enrichment for any recurrent/driver breast cancer genomic aberration within resistant or sensitive cell lines consistent with previous studies (Figure S1A) (TCGA, 2012, Meric-Bernstam et al., 2014, Xu et al., 2017). Next, we tested cell viability responses in both 2D monolayers and 3D spheroid cultures in 5 selected cell lines to demonstrate the effects of matrix attachment on response to BET inhibition (Figure 1E-G). The cell lines, HCC1954 (HER2 amplified, basal-like), BT474 (HER2+/ER+), MDAMB468 (basal-like, HER2-/EGFR amplified), SKBR3 (HER2+) and SKOV3 (HER2+, ovarian), were selected to cover different levels in the BETi sensitivity spectrum. The impact of 3D culture on cell viability was most dramatic for the most sensitive cell line, SKOV3 in which IC50 increased from ~200nM to 1.5μM (Figure S1C). The lack of genomic markers predictive of response to BETi necessitates a deeper analysis of drug response and resistance mechanisms.

We interrogated the proteomic response patterns that mediate the observed sensitivities to BETis. Using reverse phase protein arrays (RPPA), we measured the changes in 218 key oncogenic signaling molecules in response to BETis (JQ1, IBET151, IBET726, and IBET762) at two time points (24 and 48 hours) in 2D monolayer or 3D matrix-attached spheroid cultures of five cell lines (Figure 1F). RPPA monitors activity and levels of representative molecules from key pathways including PI3K, RAS-MAPK, Src/FAK, RTK signaling axes, DNA repair, cell cycle, apoptosis, immuno-oncology, and histone modifications. First, we analyzed the impact of matrix-attachment and 3D cellular organization on the proteomic landscape in the untreated state (Figure S1D). The ECM-attachment induced significant increases in EGFR/HER2 and SRC phosphorylation and lipid metabolism genes in HCC1954 and SKOV3 (SCD, FASN, p-ACC), and histone H3 levels in BT474. Significant decreases were observed in S6 phosphorylation in nearly all cell lines tested (see Figure S1D for details). Overall, the phosphoproteomic response to BET inhibition in diverse cell lines, time points, and conditions generate a comprehensive response map of the epigenetic perturbations in breast cancer cells.

Computational network modeling identifies MCL1 upregulation as an adaptive response to BET inhibition.

We analyzed the complex BETi proteomic response map using our novel network modeling strategy, termed Target Score, to identify collective adaptive responses that likely drive drug resistance and resulting drug induced vulnerabilities to combination therapies (Figure 2A-B). The algorithm quantifies a network-based Target Score for each molecular entity under the perturbations. Highest Target Scores correspond to potential adaptive responses, while the lowest Target Scores are associated with direct responses to targeted perturbations. We calculated the Target Scores for JQ1, IBET151, IBET726, and IBET762 compounds in HCC1954, BT474, MDMB468, SKBR3, and SKOV3 lines using phosphoproteomic data collected 24 and 48 hours after drug perturbation.

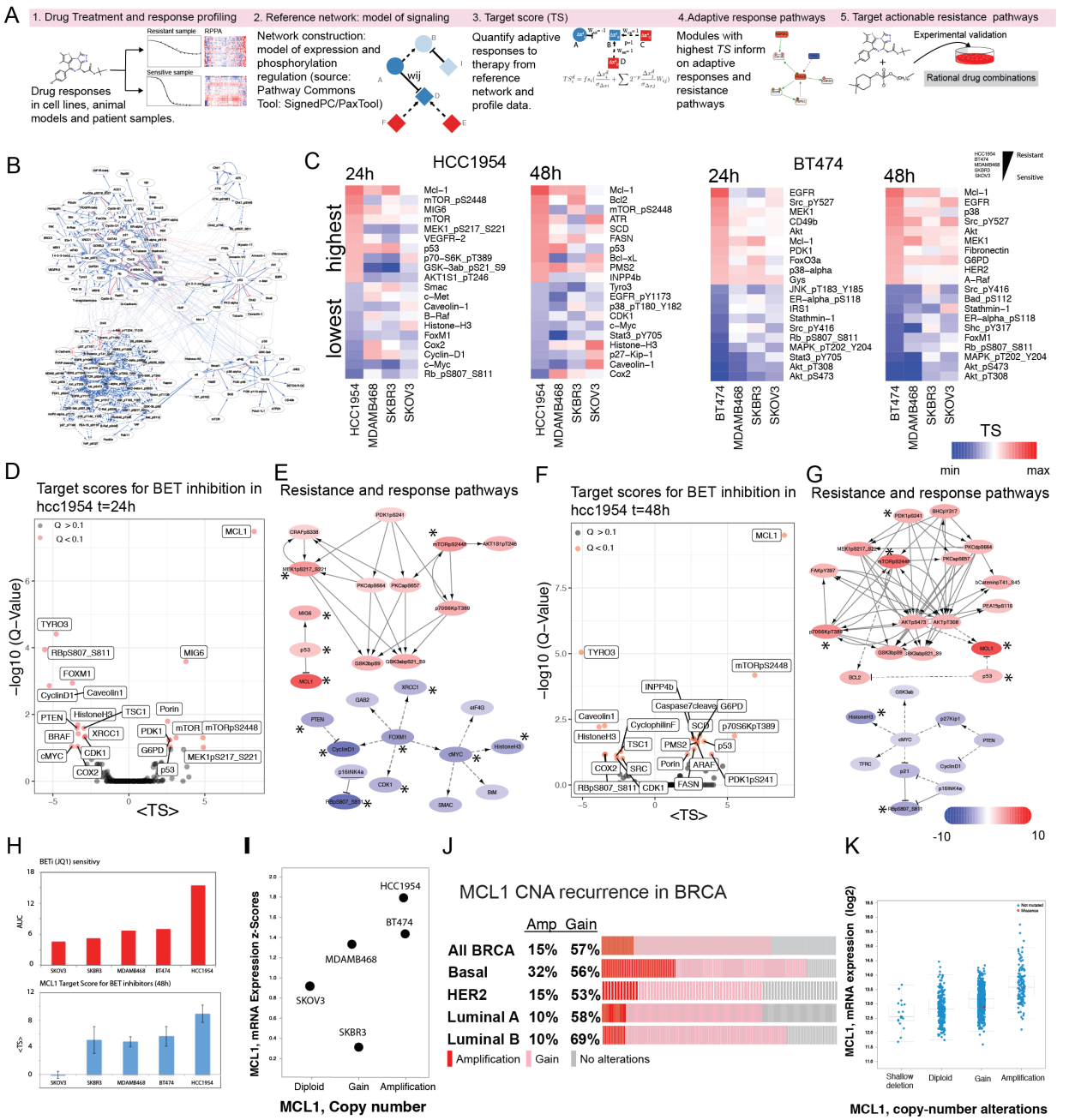

Figure 2. The computational Target Score analyses of adaptive responses to BET inhibition in breast cancer. **A**. Target Score algorithm identifies network level adaptive responses to targeted therapies. The method involves, 1. Molecular profiling of response to perturbations in samples with varying sensitivity to the perturbation agent. 2. Construction of a reference network that captures potential relations between all measured proteomic entities. 3. Quantification of a sample specific adaptation (target) score that links protein interactions to drug response on the reference network using omics-based drug response data. 4. Identification of network modules that have a significantly high target score (i.e., collectively participate in adaptive responses) in each sample. 5. Selection of actionable targets that participate in adaptive responses and experimental testing of drug combinations. **B.** Reference network model constructed for 218 phosphoproteomic entities (see methods for construction of the model). **C.** Network level adaptive responses are quantified as Target Scores using the reference network and phosphoproteomic BETi response data. The heatmaps capture the scores for 24 and 48 hours post treatment in 3D cultures. The proteomic entities with highest and lowest 10 target scores in HCC1954 (left) and BT474 (right) are displayed. The cell lines are ordered from most resistant (HCC1954 or BT474) to most sensitive (SKOV3). **D.** Meta-analysis and statistical assessment of adaptive responses (high TS) and mechanisms of action (low TS) to JQ1, IBET151, IBET726, and IBET762 in HCC1954 24 hours post treatment is shown on a volcano plot. **E.** Network modules of adaptive responses (red nodes representing

high Target Score) and mechanisms of action (blue nodes representing low Target Score) 24 hours post treatment. **F.** Meta analysis of adaptive responses in HCC1954, 48 hours post treatment. **G.** Network modules of adaptive responses and mechanisms of action for BET inhibition, 48 hours post treatment. **H.** Correlation of MCL1 Target Score (top) and BETi sensitivity (bottom). Target Score bar chart represents the mean target score across four BETis and error bars represent the 95% confidence interval. **I.** copy number and mRNA expression status of MCL1 in cell lines. **J.** The frequency of breast cancer samples with high (red) and low (pink) level copy number amplifications in MCL1. **K.** The distribution of MCL1 mRNA levels with varying MCL1 copy number status across breast cancer samples (TCGA).

Differential analysis of Target Scores for JQ1 across cell lines identified adaptive responses that are either exclusive to most resistant cell types or shared across all samples (Figure 2C). In the most resistant line, HCC1954, the anti-apoptotic protein MCL1 had the highest Target Score value in response to JQ1, in both 24 and 48 hours among the 218 phosphoproteins. In HCC1954, 24 hours after JQ1 treatment, MCL1 was followed by series of molecules downstream of receptor tyrosine kinase signaling such as mTOR, mTOR_pS2448, MIG6, MEK1/2_pS217/S221, P70S6K_pT389, GSK3**α**/**β** _pS21_S9, and AKT1S1_pT246. The enrichment of the listed proteins suggests the involvement of RTK signaling in an adaptive response to BET inhibition. At 48 hours, molecularly more diverse adaptive responses were observed as proteins involved in apoptosis (MCL1, BCL2, BCL-XL), DNA repair (ATR, PMS2), lipid metabolism (SCD, FASN), AKT/mTOR signaling (mTOR_pS2448, INPP4B) and TP53, which is mutated in HCC1954, had high Target Scores. Target Scores in BT474 carried important similarities to HCC1954. In BT474, MCL1 had a high target score (5th highest at 24 hours and the highest at 48 hours). At both 24- and 48-hour time points, high Target Scores in BT474 were associated with total protein level changes in EGFR and its downstream molecules. In conclusion, the Target Score analysis nominated upregulation of anti-apoptotic MCL1 molecule as a key adaptive response to BET inhibition exclusively in resistant lines.

We averaged Target Scores for each protein across BETis to detect a statistically robust and consistent adaptive response signature (Figures 2D, 2F). Using a bootstrapping based statistical assessment method with randomized protein labels, we eliminated high Target Scores that are solely driven by network connectivity biases without a significant input from cell type-specific response data (FDR-adjusted $p > 0.1$, see methods). MCL1 (at both 24hr and 48hr), MIG6 (at 24hr), and mTORpS2448 (at 48hr) had the most significant (Padj < 10e-4) and highest target scores in HCC1954. At both time points, various markers of AKT (P70S6K_pT389, PDK1_pS241, mTOR_PS2448), MAPK (MEK1/2_pS217/S221), and lipid metabolism (SCD and FASN) pathways had high target scores. The FDR-adjusted p-values decreased to less than 0.1 at 48 hours particularly for the lipid metabolism proteins SCD and FASN. MCL1 Target Score followed a near monotonously decreasing trend with increasing sensitivity to JQ1 assuming the lowest Target Score in SKOV3 line and highest Target Score in HCC1954 (Figure 2H, Figure S2). The trend suggests MCL1 upregulation is correlated with resistance to BET inhibition. Although mTOR_pS2448 had high target scores in HCC1954, there was no correlation between Target Scores and sensitivity to JQ1 across cell lines. In conclusion, the integrated statistical analysis results for JQ1, IBET151, IBET726, and IBET762 were consistent with JQ1-focused analyses particularly in nomination of MCL1 as a key driver of adaptive responses (Figure S2).

The lowest Target Scores correspond to network level responses that are likely associated with action mechanisms of the BETis. In both HCC1954 and BT474, cell cycle proteins RB1_pS807, CyclinD1, c-Myc, and p27/Kip1 had the lowest target scores (Figure 2E-G, Figure S2). Interestingly, in BT474, phosphorylation of MAPK and AKT pathway members were also marked with low Target Scores despite increases in total levels and corresponding high Target Scores of the total protein expression in EGFR, AKT and MAPK pathways, suggesting the existence of alternative routes downstream of EGFR/HER2 in BT474. Consistent with existing literature, our

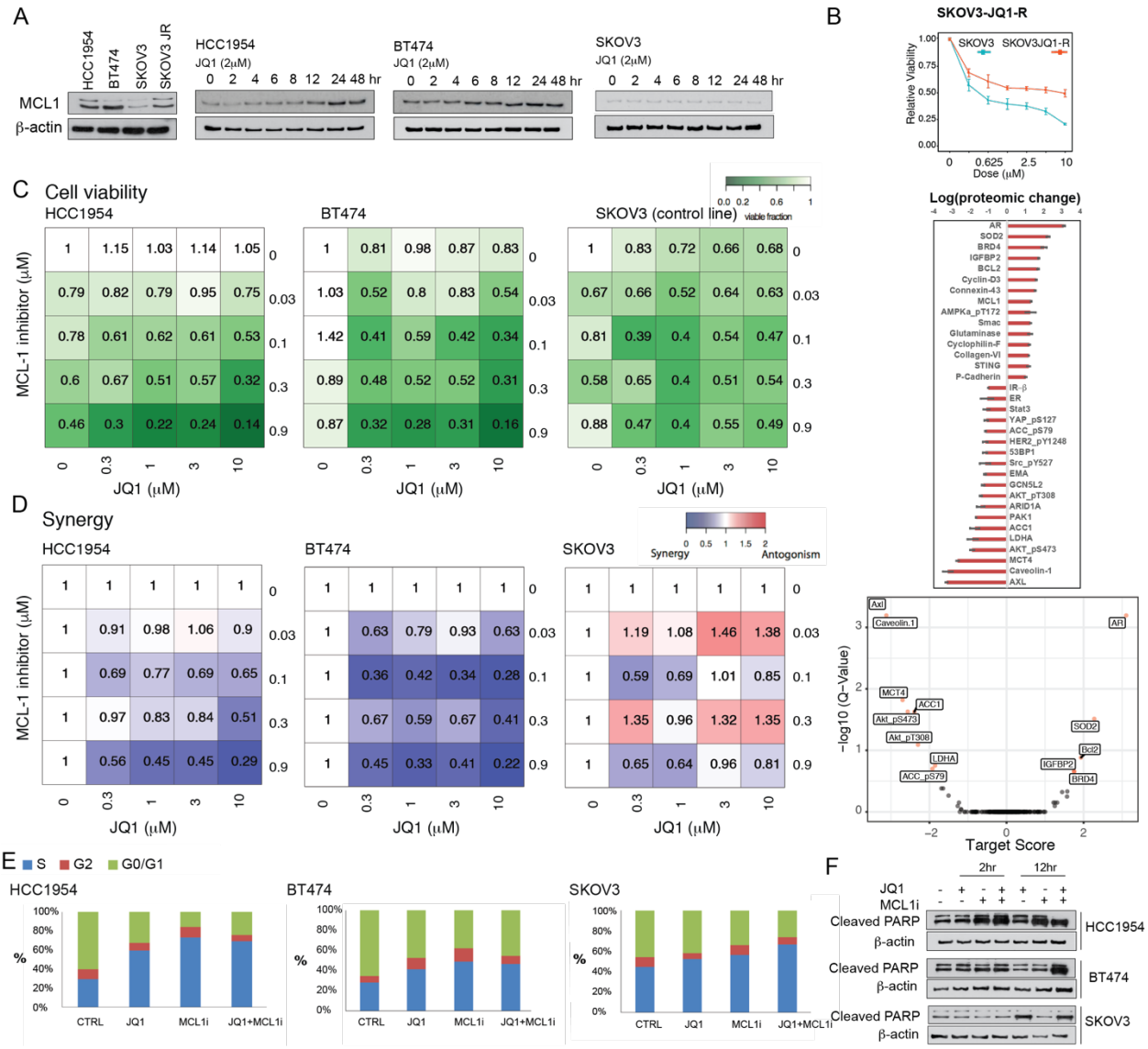

Figure 3. Synergistic responses to combination of BET and MCL1 inhibitors in breast cancer. A*. MCL1 protein expression in drug naive BETi resistant (HCC1954, BT454, SKOV-JQ1-R) and BETi sensitive (SKOV3) cells (left). MCL1 protein level changes in response to BET inhibition (2μM of JQ1, 0 to 48 hours).* ***B.*** *Long term adaptive responses and acquired resistance to JQ1. Cell viability responses of SKOV3-JQ1-R and SKOV3 to increasing doses of JQ1 (top). The highest amplitude phosphoproteomic changes in response to JQ1 in SKOV-JQ1-R cells (center). The Target Score analysis of JQ1 response in SKOV3-JQ1-R determines the network level adaptive responses (bottom).* ***C.*** *Cell viability response to inhibitors of MCL1 (S63845) and BET in HCC1954, BT474 and SOKV3 cells in 3D spherical cultures supplemented with 2% matrigel.* ***D.*** *The synergistic drug interactions between JQ1 and S63845 are quantified using the Bliss independence method.* ***E****. The shift in cell cycle stage distribution in HCC1954, BT474 and SKOV3 in response to JQ1 (2μM) and S63845 (0.3μM) combination 48 hours post treatment are quantified using flow cytometry.* ***F****. The western blotting analysis of cleaved PARP levels monitors apoptotic response to JQ1 and S63845, 2 and 12 hours post treatment.*

differential and statistical analyses of Target Scores suggest that BETis act through reduction of cell cycle progression (Zhang et al., 2019, Sahni et al., 2016). The analysis of MCL1 copy number and transcriptomic status provides orthogonal evidence on roles of MCL1 in drug resistant cells (CCLE data source, Barretina et al., 2012). MCL1 is copy-number-amplified and mRNA overexpressed in the resistant lines HCC1954 and BT454 (Figure 2I). MCL1 is copy-number-

gained and has intermediate mRNA expression in the MDAMB468 line, which has a comparable but lower JQ1 resistance. More sensitive cell lines, SKBR3 and SKOV3, have low mRNA expression and/or diploid copy number states for MCL1. Indeed, MCL1 is one of the most recurrent copy-number-altered oncogenes in breast cancers (Berger et al., 2018). High level copy number amplifications and low-level gains in the MCL1 locus are observed in 15% and 57% of breast cancer cases in the TCGA cohort, respectively (Figure 2J). Aberrations in MCL1 are enriched in the aggressive basal subtype with 32% of cases being copy-number-amplified. The HER2+ subtype is intermediate with a 15% MCL1 amplification frequency followed by less frequent aberrations in the luminal subtypes (10%). Despite the well-established role of MCL1 amplifications as breast cancer drivers, little is known of the significance of low-level gains, which lead to relatively high mRNA expression compared to MCL1 diploid cases (Figure 2K). Motivated by the strong evidence from Target Score analysis, the orthogonal evidence from genomic analysis, and driver roles of MCL1 in breast cancer, we decided to experimentally test the combined effect of BET and MCL1 inhibition in breast cancer cells, particularly those that are most resistant to BET inhibition where effects are most likely to be manifest.

MCL1 protein levels inversely correlate with BETi sensitivity

We profiled MCL1 levels in BET-inhibitor-treated and drug-naive cells with varying JQ1 sensitivity (Figure 3A). As it was expected from the copy number and transcriptomic states, HCC1954 and BT454 cells (MCL-1 amplified) expressed substantial levels of MCL1 protein in their drug-naive state, whereas SKOV3 cells (MCL1 wild-type) had lower MCL1 protein expression. SKOV3-JQ1R cells, which acquired resistance to BET inhibition through chronic exposure to increasing doses of JQ1 for > 3 months, had upregulated MCL1 levels compared to drug naive SKOV3 cells. The increased MCL1 expression in SKOV3-JQ1R provides further evidence that MCL1 has a role in resistance to the BETi. In BT454 and HCC1954, treatment with JQ1 led to time dependent increase of MCL1 levels as shown by western blots. MCL1 protein level was not upregulated in the BETi sensitive SKOV3 cells in response to short term (48 hours) BETi treatment. Interestingly, RPPA and Target Score analysis of SKOV3-JQ1-R cells revealed a more complex adaptive response landscape involving other oncogenic proteins such as androgen receptor and Superoxide dismutase 2 (SOD2) although both MCL1 and BCL2 were among the most upregulated proteins (Figure 3D). The comparison of short versus long term adaptive responses demonstrates the need for temporal molecular profiling and differential therapeutic approaches across disease progression. The molecular validation of MCL1 upregulation in cell lines with de novo or acquired resistance to BET inhibition provides an additional rationale for testing responses to combined inhibition of BET and MCL1 proteins.

BET and MCL1 inhibitors are synergistic in breast cancer cells

Guided by the computational predictions and genomic evidence, we treated BETi refractory HCC1954 and BT454, and relatively sensitive SKOV3 cells with combinations of JQ1 and highly selective MCL1 inhibitor (MCL1i) S63845 (Kotschy et al., 2016) (Figure 3). Despite being an ovarian cancer line, SKOV3 line is selected as the control line to decode events exclusive to more resistant cells for the following reasons. First, SKOV3 originates from a patient with serous adenocarcinoma, an ovarian cancer subtype with similarities to basal-like breast cancers (TCGA, 2012). Second, SKOV3 line also carries major genomic similarities to breast cancers (e.g., TP53-null, HER2 amplified, PIK3CA-mutated).

We measured the cell viability responses to the combination of MCL1 inhibitor (S63845) and BETi, (JQ1) (Figure 3B) in cells with varying BETi sensitivity. Consistent with our previous experiments, cell viability was not affected by increasing doses of JQ1 in HCC1954 and BT454. Yet, we

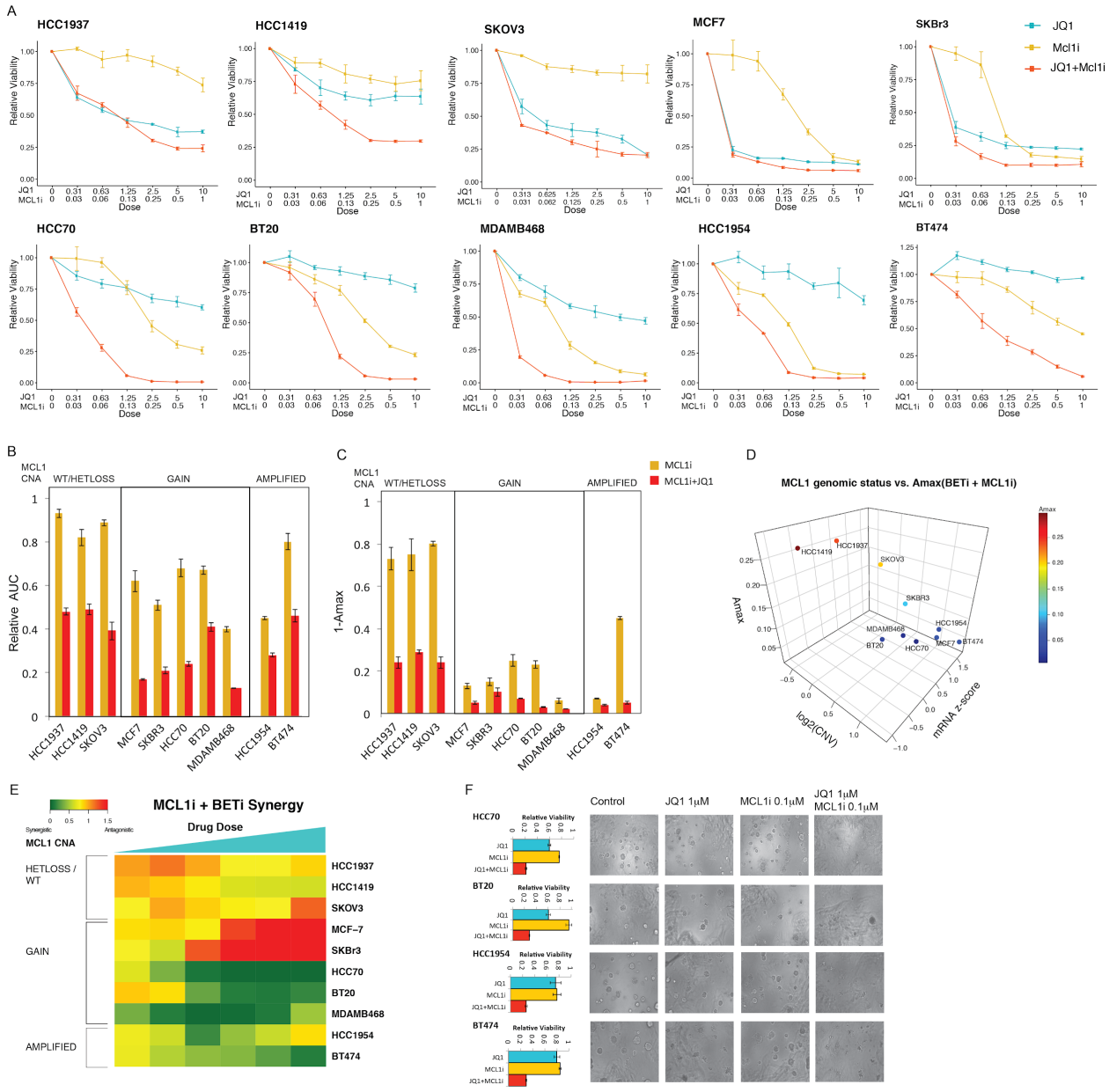

Figure 4. Molecular determinants of responses to MCL1 and BET inhibition. A. *Dose-response curves of BETi (JQ1) and MCL1i (S63845) in breast and ovarian cancer cell lines.* ***B****. The normalized AUC (AUC/AUC$_{100\% \text{ viability}}$) for S63845 and combination of JQ1 and S63845. Cell lines are classified according to MCL1 copy number status.* ***C.*** *Amax (response at maximum dose) for S63845(1μM) and combination of JQ1 (10μM) and S63845 (1μM), classified according to MCL1 copy number status.* ***D.*** *The relation between combination therapy Amax, MCL1 mRNA levels and MCL1 copy number status as profiled in CLLE project for all tested cell lines.* ***E.*** *The synergy, additivity and antagonism between JQ1 and S63845 are quantified with Bliss independence score for increasing doses of drugs for cell lines with varying MCL1 copy number status.* ***F.*** *Cell viability responses to JQ1 (1μM) and S63845 (0.1 μM) in 3D cultures of select cell lines treated with JQ1 (1μM) and S63845 (0.1 μM). Images are collected 72 hours after drug treatment.*

observed a substantial response to MCL1 inhibition (0.9 μM S83645) in HCC1954, with a 54% reduction of cell viability, while BT474 was relatively more resistant with 13% reduction. Both cell lines were highly responsive to combination treatment as evidenced by more than 80% reduction

in cell viability when JQ1 and S83645 were introduced at 10 and 0.9 μM, respectively. In contrast, SKOV3 showed a relatively higher response with 30% reduction to the 1μM JQ1 treatment, and was not responsive to the S83645 or the combination. We quantified the synergy between BET and MCL1i using Bliss independence metric, where lower independence scores suggest synergy and higher values suggest antagonism (Figure 3C). As a subjective but highly strict criterion, we assume a strong synergy between two compounds when Bliss score is less than 0.5. In both BT474 and HCC1954, the combination was highly synergistic in diverse doses. In HCC1954, the synergies were stronger in increasing doses reaching to a Bliss score of 0.29 at the highest dose. The two drugs were highly synergistic for all doses of JQ1 and MCL1i in BT474, with Bliss scores below 0.5 at 0.1μM S83645 and 0.3μM JQ1. The relatively low synergy and additive characteristics (Bliss scores 0.8 to 1.0) in low drug doses in HCC1954 can be attributed to the relatively high sensitivity of HCC1954 to MCL1i as a single agent, which hinders detection of synergistic responses to the combination. In SKOV3, no consistent synergy was observed and the two compounds were antagonistic in multiple dose configurations with Bliss scores as high as 1.45. Thus, we validated the Target Score based predictions on co-targeting MCL1 and BET.

To determine the mechanisms underlying synergy, we measured the effects of BET and MCL1 targeting on cell cycle progression and apoptosis. Cell cycle progression and arrest was quantified with DNA content measurements 48 hours after drug perturbations using flow cytometry (Figure 3E). Consistent with the Target Score calculations, which suggested a reduction of cell cycle pathway activities, JQ1 induced an S-phase cell cycle arrest in all samples. In HCC1954, the S-phase population was enriched from 30% to 59.8% upon 2μM JQ1 treatment. In BT474, we observed a similar but intermediate increase in the fraction of cells in S-phase (from 28% to 41.5%) upon JQ1 treatment. The shift, which was induced by JQ1 in the S-phase population was lowest in SKOV3, with an increase from 44.8% to 52.4% after 48 hours. Next, we monitored the apoptotic responses with the detection of PARP cleavage (Figure 3F). We observed that 12 hours of JQ1 treatment at 2μM induced PARP cleavage in SKOV3 but not in the drug-resistant HCC1954 and BT474. The observed cell cycle arrest across all cell lines and the lack of apoptotic cells in drug resistant cells explain the static cell viability profiles in response to monotherapy in HCC1954 and BT474. Treatment with the single agent S83645 at 0.3μM induced PARP cleavage in HCC1954 but not in the SKOV3 and BT474. The cell viability assays also suggested that BT474 and SKOV3 cells were refractory to single-agent MCL1 inhibition. The JQ1 and S83645 drug combination, induced PARP cleavage in all tested cell lines, particularly in HCC1954 and BT474. The apoptotic shift and reduced cell count in response to JQ1 and S83645 combination provides strong evidence that JQ1-induced MCL1 activity plays a major role in driving resistance to BET inhibition in breast cancer (Figure 3E-F). This finding also further validates the utility of predictions from the Target Score algorithm.

MCL1 copy number status is a predictor of response to co-targeting MCL1 and BET

Next, we investigated the predictors of response to MCL1 inhibition alone or in combination with BET inhibition. We focused on MCL1 copy number status motivated by the computational predictions and the subsequent experimental validation of the drug combination in MCL1 amplified cell lines.

To investigate the role of MCL1 amplification, we tested the effect of MCL1 and BET inhibitors on cell viability in 10 cell lines (9 breast lines and SKOV3) with varying cancer subtypes and genomic backgrounds (Figure 4A). The response to therapy was quantified and evaluated by (i) normalized area under the curve ($nAUC = AUC_{observed}/AUC_{100\% \text{ viability at all doses}}$) for drug efficacy across multiple doses, (ii) A_{max} for responses at high doses, and (iii) drug synergy (Bliss independence) for drug interactions. The weakest responses to MCL1 inhibition were observed in HCC1937, HCC1419

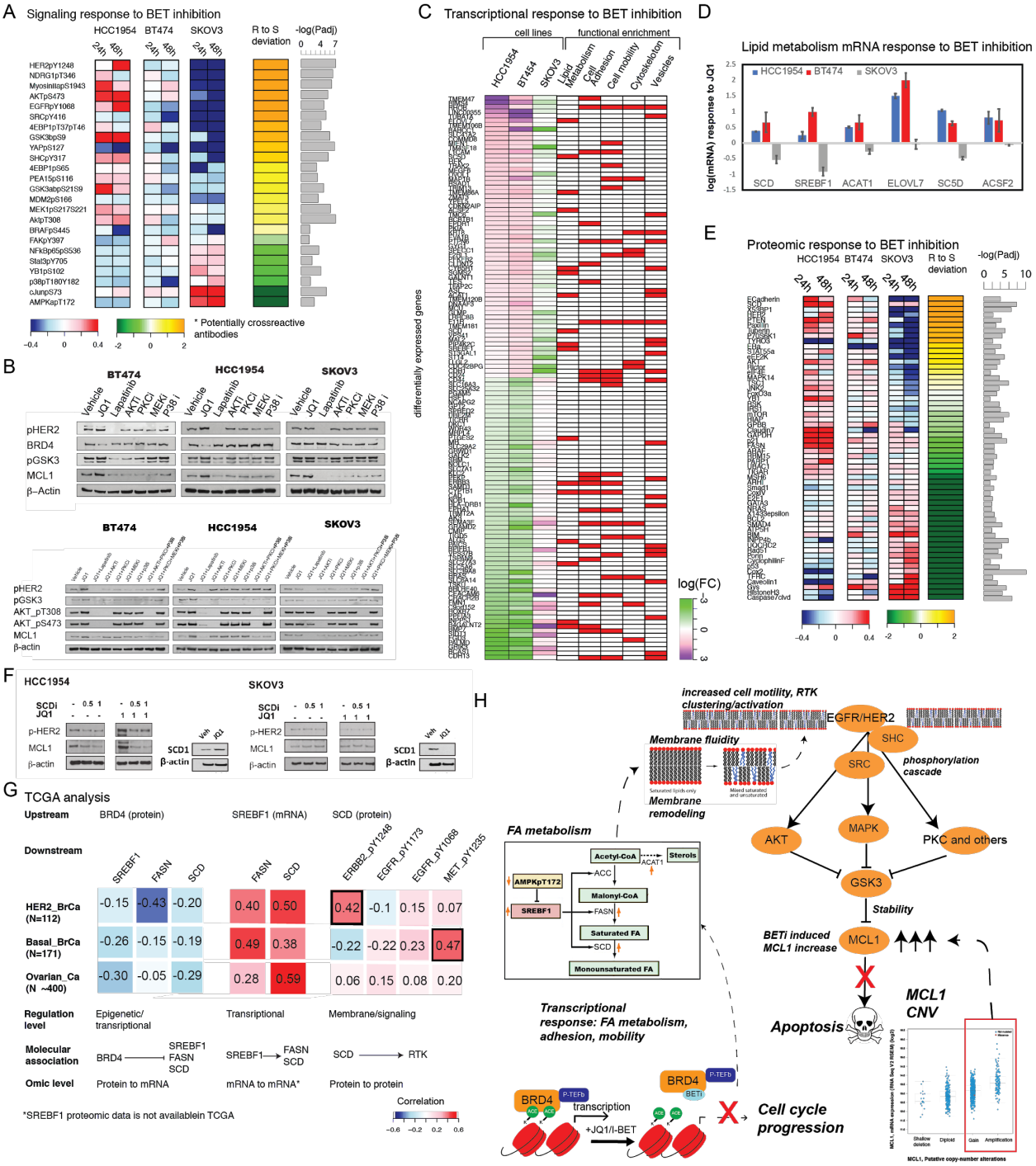

Figure 5. Molecular mechanisms of response to combined BET and MCL1 targeting. A. *Differential analysis of phospho-proteomic response to BETis in resistant (HCC1954, BT474) and sensitive (SKOV3) cells. The heatmap represents the average log fold difference (log[$X_{perturbed}/X_{unperturbed}$]) across four BETis (JQ1, IBET151, IBET726 and IBET762). "R to S deviation" is the difference of fold changes between resistant (HCC1954 and BT474) and sensitive (SKOV3) cells (see methods for RPPA analysis).* ***B.*** *MCL1, AKT signaling and HER2 activity changes in response to pathway and BET inhibition in HCC1954, BT474 and SKOV3 are measured. Responses to pathway inhibitors applied as single agents (top panel) and combinations with JQ1 are monitored to demonstrate the role of signaling pathways linking BET and MCL1 activity.* ***C.*** *Differential analysis of transcriptomic responses to BET inhibition in resistant vs. sensitive cell lines. The first three columns in the heatmap demonstrates fold changes of mRNA species that change in opposite directions in resistant versus sensitive lines. The red/white columns on right represent involvement of each*

differentially expressed gene in different molecular processes according to a GO-term enrichment analysis. ***D.*** *Transcriptomic responses in key genes of the lipid metabolism pathway as identified by the differential response analysis.* ***E****. Differential total protein analysis is performed with focus on only total protein changes.* ***F****. The analysis of SCD, MCL1 and p-EGFR/p-HER2 levels in response to inhibitors of BET (JQ1 at 1μM) and SCD (A939572). The SCD, MCL1 and p-EGFR/p-HER2 levels are measured 48 hours after drug perturbation in HCC1954 and SKOV3 cells.* ***G.*** *Correlation analysis of proteomic and transcriptomic levels involved in the proposed associations linking BET to EGFR/HER2 within HER2+, basal and ovarian cancer patients. Each analysis reflects a particular step in the pathway -i.e., BET to fatty acid synthesis, fatty acid enzymes to RTK signaling. All correlations are in the range of -0.5 to 0.5, consistent with relatively low correlations observed between omic entities in other TCGA studies. As a reference, the average correlation between mRNA and protein levels of a given gene is estimated within a range of 0.3-0.6 across whole genome in different studies (Liu et al., 2016, and Gry et al., 2009).* ***G.*** *The proposed mechanism of BET induced vulnerability to combined BET and MCL1 targeting in the context of MCL1 chromosomal amplifications or gains based on the integrated multi-omics, network and perturbation analyses. The marked genes and proteins are identified and validated in molecular perturbation response analyses.*

---

and SKOV3, which have either diploid or single copy of MCL1 gene (Figure 4B-C). Normalized AUC (mean=0.93) and Amax (mean =83%) were significantly higher in HCC1937, HCC1419 and SKOV3 compared to other lines (p-val=0.007, H_o: $nAUC^{MCL1i}(MCL1_{wt/hetloss}) = nAUC^{MCL1i}(MCL1_{gain/amp})$; p-val<0.001, H_o: $A_{max}^{MCL1i}(MCL1_{wt/hetloss}) = A_{max}^{MCL1i}(MCL1_{gain/amp})$). Cell lines with either low level gain or high-level amplification in MCL1 gene were more responsive to MCL1 inhibition with effective eradication of tumor cells (Amax μ= 0.19) at high doses and significantly low AUC (μ= 0.59). The combination of MCL1 and BETis augmented cell viability responses in all tested cell lines. The mean nAUC across cell lines with MCL1 copy number alterations was reduced from 0.59 for MCL1 mono-therapy to 0.33 for the combination. For cell lines with wild type or heterozygous loss of MCL1, the nAUC was reduced from 0.90 to 0.60 with combination therapy. A more dramatic response was observed in Amax. In cells with MCL1 amplification, a near-complete eradication of tumor (Amax μ= 0.05) was observed in contrast to cell lines carrying no MCL1 amplification (Amax μ= 0.36) (Pval < 0.001, H_o: $A_{max}^{MCL1i+JQ1}(MCL1_{wt/hetloss}) = A_{max}^{MCL1i+JQ}(MCL1_{gain/amp})$). Next, we analyzed the association between MCL1 copy number status, mRNA levels, and Amax for response to JQ1 and S63845. The copy number and mRNA expression values for each cell line were extracted from the CCLE database. The analysis demonstrates MCL1-low (mRNA and copy number) cell lines are clearly separated in their response to the combination from the MCL1-high cell lines, which have much lower Amax (i.e., higher sensitivity) (Figure 4D). In a parallel analysis of 10 cell lines, we did not observe any significant enrichment of increased MCL1i and/or MCL1 + BETi sensitivity in tumors with other recurrent oncogenic aberrations (Figure S4). The separation based on MCL1 copy number and mRNA levels suggest a clear association with MCL1 levels and response to the drug combination.

Next, we computed drug synergy using the Bliss independence score for all drug doses across all cell lines and detected three clusters with distinct JQ1 and MCL1i synergy (Figure 4E). The first cluster (HCC1937, SKOV3, HCC1419) consisted of MCL1 inhibitor resistant lines and is characterized by additive drug interactions between BET and MCL1 inhibitors (0.5 < Bliss score < 1.0). In the second cluster (SKBR3, MCF7), an antagonistic interaction (Bliss score > 1.0), which can be attributed to the high efficacy of JQ1 as a single agent, was observed. In the third cluster (HCC70, BT20, MDAMB468, HCC1954, and BT474) a strong synergy was observed with Bliss synergy scores below 0.5. The cells in the third cluster were highly resistant to JQ1 and also carry MCL1 copy number gains. Finally, we confirmed that synergistic interactions between JQ1 and S63845 were also preserved in 3D spheroid cultures (Figure 4F). In summary, a robust and strong synergy exists between targeting MCL1 and BET in the BETi resistant and MCL1 amplified context.

We conclude, based on the drug responses and synergies across cell lines with varying MCL1 levels, MCL1 copy number status is a predictor of response to the drug combination that could potentially be translated to the clinic to identify patients likely to benefit.

BETi induced MCL1 upregulation is mediated by EGFR/HER2 signaling activity

To elucidate signaling mechanisms underlying adaptive MCL1 protein upregulation in the presence of MCL1 amplification and BETi resistance in breast cancer, we searched for the phosphorylation cascades that links BET inhibition to MCL1 accumulation and subsequent apoptotic evasion. We quantified differential phosphorylation of each protein based on RPPA data from resistant and sensitive lines (Figure 5A). The most differentially phosphorylated proteins were predominantly driven by the difference between the most resistant line HCC1954 and the sensitive line SKOV3. The analysis revealed enrichment of the HER2/EGFR downstream signaling in BETi resistant cells as phosphorylation of HER2, EGFR, SHC, SRC, AKT, GSK3**α**/**β**, MEK1/2 and 4EBP1 were increased in response to BET inhibition in HCC1954 but not in SKOV3. In addition to the RTK and downstream signaling, we observed increased phosphorylation of Myosin II and NDRG1. Based on the results, we hypothesized that BETi induced MCL1 increase and subsequent apoptosis evasion through HER2/EGFR activation and subsequent downstream signaling.

To test this hypothesis and generate causal links from HER2/EGFR signaling to MCL1 upregulation, we performed perturbation experiments coupled to MCL1 and signaling profiling (Figure 5B). First, we treated HCC1954, BT474, and SKOV3 cells with inhibitors of BET (JQ1), EGFR/HER2 (lapatinib), AKT (MK-2206), P38/MAPK14 (Doramapimod), PKC (Dequalinium Chloride), and MEK1/2 (trametinib) applied as single agents. In BT474 and HCC1954, both MCL1 and GSK3**α**/**β**_pS9/S21 levels were increased in response to JQ1 and substantially decreased in response to lapatinib. Inhibitors of downstream effector molecules (AKT, MAPK14, MEK1/2, PKC) had either partial or no impact on MCL1 levels. To test whether the inhibition of individual signaling routes downstream of EGFR/HER2 can reverse adaptive responses to BET inhibition, we treated the cells with combinations of pathway and BET inhibitors. In BT474 and HCC1954; MCL1, AKT_pS373/pT308 and GSK3**α**/**β**_pS9/S21 levels decreased in response to lapatinib and JQ1 combination suggesting HER2/EGFR inhibition reverses adaptive responses to BET inhibition. In contrast, MCL1 and GSK3**α**/**β** _pS9/S21 levels were modestly increased in response to paired combinations of JQ1 with all other agents (i.e., inhibitors of AKT, MEK1/2, PKC and MAPK14/P38) suggesting each signaling axis has limited participation in the BETi adaptive response or alternatively that inhibition of one mediator results in activation of the other pathways. Indeed, adaptive responses were blocked only when a cocktail of three signaling inhibitors was combined with JQ1 (i.e., combination of JQ1 with cocktails of PKCi+P38i+AKTi or PKCi+P38i+MEK1/2i). In HCC1954 and BT474, the molecular responses to combinatorial perturbations suggest that EGFR/HER2 activation is necessary and sufficient for increased MCL1 in HCC1954 and BT474. However, the downstream signaling cascades are highly redundant such that none of the tested inhibitors other than lapatinib could completely block the adaptive response to BET inhibition, suggesting that parallel routes downstream of EGFR/HER2 converge to regulate MCL1 levels.

A BETi induced transcriptional program activates HER2/EGFR through membrane reorganization

To identify potential links between BET inhibition and EGFR/HER2 activation, we measured transcription and total-protein changes in response to BET inhibition. Transcriptomic responses are profiled with 1μm JQ1 treatment for 48h in HCC1954, BT474 and SKOV3 cells with mRNA sequencing (Figure 5C). The mRNA analysis identified 127 differentially responding transcripts in

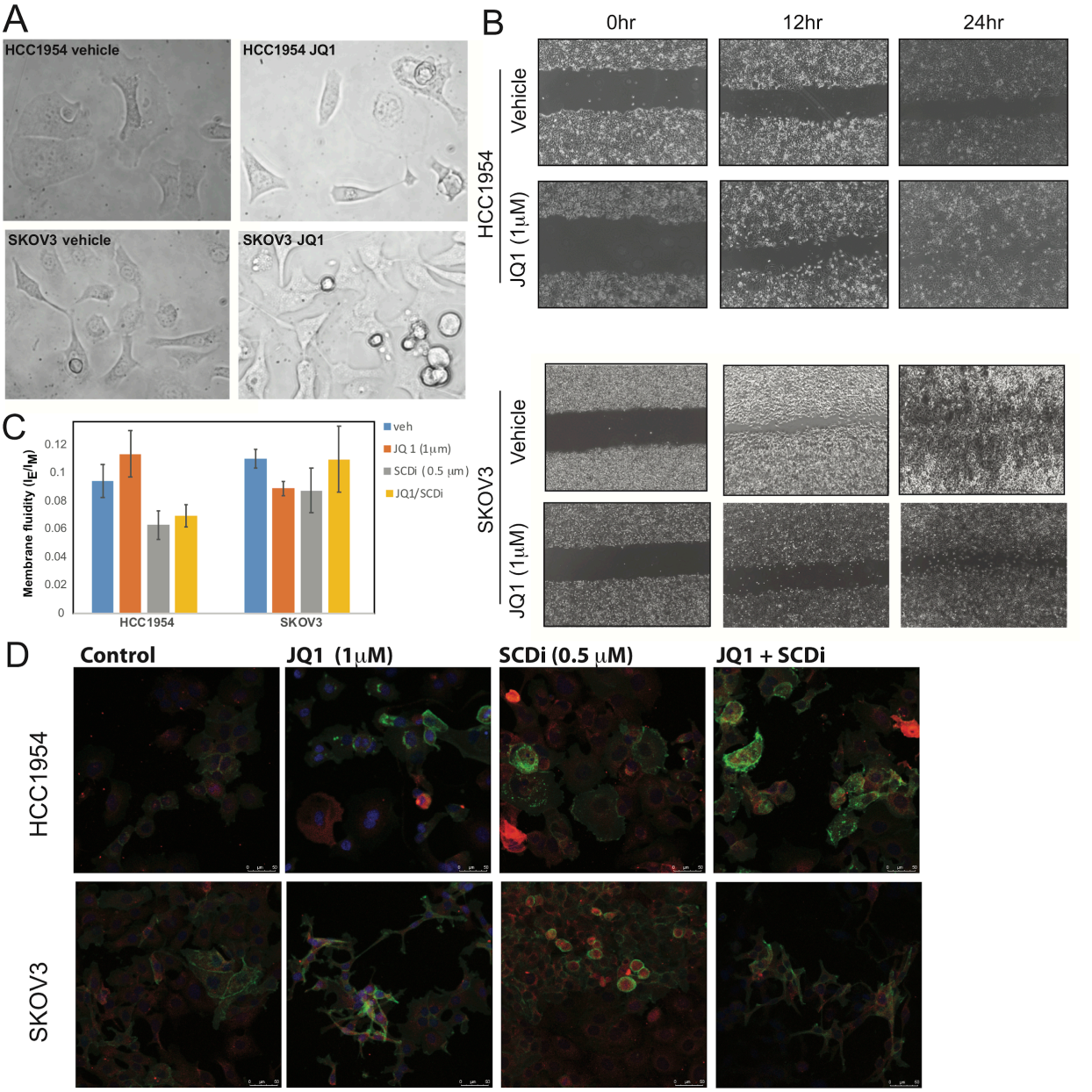

Figure 6. Phenotypic responses to BET inhibition in resistant and sensitive cells. A. *representative images (20X, brightfield) of cellular morphology changes in response to BETi in JQ1 resistant (HCC1954) and sensitive (SKOV3) cells.* ***B****. The BETi induces increased motility of HCC1954 (top) and no substantial difference in SKOV3 (bottom) as monitored across time points with a wound scratching assay.* ***C.*** *Drug induced changes in membrane fluidity in HCC1954 and SKOV3 cells based on fluorescent lipophilic pyrene probes that are enriched in excimer state (emission l = 470nm) with increasing membrane fluidity and enriched in monomers (emission l= 400nm) with decreasing membrane fluidity. The membrane fluidity is increased with JQ1 treatment in HCC1954 and decreased in SKOV3. SCD inhibition decreases membrane fluidity as expected.* ***D.*** *The representative images of HER2 localization changes in response to BET and SCD inhibition in HCC1954 and SKOV3 cells. Images are collected using fluorescent confocal microscopy. BETi induced increased and polarized fluorescence signals from HER2 (green) in HCC1954. Whereas the HER2 signal was unchanged in response to therapy in SKOV3 cells. SCD inhibition induced punctuated HER2 patterns in cell membrane of HCC1954, possibly corresponding to disruption of cell membranes due to increased lipid saturation.*

HCC1954/BT474 versus SKOV3. A GO-term analysis of the differentially expressed genes identified 85 statistically significant pathways with enrichment of biosynthetic pathways

particularly lipid metabolism, cell adhesion, and motility in resistant lines (suppl. table 1). The enrichment profiles suggest that the BETi transcriptional program is associated with lipid bilayer cell membrane changes in drug resistant samples. Indeed, stearoyl-CoA desaturase (SCD), which catalyzes the rate limiting step in monounsaturated fatty acid (MUFA) synthesis and regulates lipid membrane fluidity in cells (Röhrig et al., 2016, Stubbs et al., 1984, and Roongta et al., 2011), was part of 43 out of 85 significant pathways. In addition to SCD, other key lipid metabolism enzymes, including SREBF1 - a master transcription factor that regulates expression of key fatty acid enzymes (e.g., SCD, FASN), ELOVL7, SC5D, ACSF2, and ACAT1 are differentially overexpressed in response to BET inhibition in resistant cells (Figure 5C-D). Moreover, differential analysis of total protein expression suggests the involvement of cell adhesion and fatty acid metabolism in BETi response, with E-cadherin and SCD as the highest-ranked differentially expressed genes in resistant cells (Figure 5E). BETi also differentially increased MyosinII_pS1943 and decreased AMPKa_pT172 supporting the hypothesis that BET inhibition alters motility and lipid metabolism, respectively.

Motivated by the roles of SCD as a rate limiting step in monounsaturated fatty acid formation and a regulator of membrane fluidity, we focused on SCD involvement in modulating EGFR/HER2 activity and MCL1 protein levels in response to BET inhibition. The treatment of HCC1954 cells with the SCD inhibitor (SCDi, A939572) decreased both p-HER2/EGFR and MCL1 levels, suggesting a role of SCD upstream of the HER2/EGFR - MCL1 signaling axis (Figure 5F). To identify whether the BETi-induced MCL1 accumulation depends on SCD, we treated HCC1954 with JQ1 and A939572. Both HER2 phosphorylation and MCL1 were decreased upon combined BET and SCD inhibition suggesting that SCD inhibition can reverse adaptive responses to BET inhibition. In conclusion, BETi induced SCD transcription and activity is an intermediate event between BET inhibition and HER2/EGFR to MCL1 signaling axis.

Next, we asked whether the relationships between BET inhibition, fatty acid synthesis and RTK activation, which we have demonstrated that leads to MCL1 upregulation in cell lines, were also valid across larger patient cohorts. Using TCGA breast and ovarian cancer data, we performed a correlation analysis of mRNA and protein levels in therapy naive ovarian, HER2+ breast and basal breast tumors (Figure 5G). We calculated correlations between (i) BRD4 protein versus key partners of fatty acid synthesis pathway (SREBF1, FASN, SCD) to profile the impact of BRD4 on transcription of fatty acid pathway members, (ii) mRNA levels of SREBF1 versus SCD and FASN to capture the transcriptional activity of SREBF1, which is the key transcription factor regulating expression of fatty acid synthesis enzymes, and (iii) protein levels of SCD and FASN enzymes versus p-RTK (HER2, EGFR, MET) to capture the effect of fatty acid synthesis pathway on RTK signaling. In all cancer types, BRD4 protein level was negatively associated with SREBF1, SCD and FASN ($-0.43 < R < -0.05$). This was consistent with the increased expression of fatty acid synthesis genes with BET inhibition in HCC1954 cells. SREBF1, for which no proteomic data was available, was quantified based on mRNA levels. Consistent with prior reports on the role of SREBF1 on transcription of lipid metabolism genes (Kim et al., 1996), SREBF1 and the two key enzymes FASN and SCD are strongly correlated ($0.28 < R < 0.59$). RTK activation was analyzed based on available p-RTK measurements (i.e., p-HER2, p-EGFR and p-MET). The relation between SCD, the rate limiting enzyme in fatty acid synthesis, with RTK expression was highly context dependent: In HER2+ cells, SCD was highly correlated with p-HER2 ($R=0.42$) but not with p-EGFR or p-MET. In basal cancers, in which HER2 activity is not a driver, the correlation between SCD and p-HER2 was diminished, while a high correlation between SCD and p-MET was observed ($R=0.47$). In ovarian cancers, weak correlations between SCD and the measured p-RTK species were observed but no individual RTK demonstrated a strong association ($0.06 < R < 0.2$). We did not observe similar associations between BRD4 and fatty acid metabolism in luminal A and B breast tumors. Thus, TCGA analysis suggests that the mechanistic link between

BRD4, fatty acid metabolism and RTK activation is relevant across a large fraction of HER2-amplified and basal breast cancers and to a lesser degree, serous ovarian cancers.

Finally, we profiled BETi induced phenotypes which are potentially associated with the transcriptomic and proteomic responses in resistant lines. In HCC1954 but not in SKOV3, BETi treatment (48 hours,1μM JQ1) induced morphology changes involving a transformation from a less structured and spread form to a more ordered and contracted state, while no substantial difference was observed in SKOV3 (Figure 6A). Wound scratch assays in monolayer cultures showed that 24 hours after BET inhibition (1μM JQ1) cell motility increased in BETi resistant cells (HCC1954) but not in sensitive cells (SKOV3) (Figure 6B). Consistent with BETi induced SCD upregulation, HCC1954 membrane fluidity was increased upon JQ1 treatment (48 hours,1μM JQ1) as quantified by the ratio of monomer to excimer fluorescence of lipophilic pyrene probes (Abcam), which undergo excimer formation with increasing membrane fluidity. SKOV3 membrane fluidity was decreased in response to BETi consistent with the observed cell motility decrease. As expected, SCDi decreased membrane fluidity in both HCC1954 and SKOV3. We monitored EGFR/HER2 localization changes after JQ1 and SCDi treatment for 48 hours in HCC1954 and SKOV3 cells (Figure 6D). In drug resistant HCC1954 cells, HER2 protein molecules were upregulated and polarized on the cell membrane after JQ1 treatment. SCDi treatment induced localization of HER2 molecules in vesicle-like structures visualized as fluorescent spots both on the surface and cytoplasm of HCC1954 cells. In contrast to JQ1, SCD inhibition, however, did not generate a polarized HER2 localization on the cell surface. After combined JQ1 and SCDi treatment, cell morphology was similar to cells that were treated with SCDi alone, suggesting that SCD inhibition can rescue the effect of JQ1 on morphology. In contrast, no change in HER2 localization was observed in BETi sensitive cells (SKOV3), upon BETi or SCDi treatment. We conclude that BET inhibition induces membrane remodeling including cell morphology, motility, fluidity and receptor tyrosine kinase localization changes associated and consistent with the observed molecular changes in drug resistant cells.

Discussion

We demonstrated that BETis induce an anti-apoptotic adaptive response marked by MCL1 upregulation and that combined inhibition of BET and MCL1 proteins are synergistic in cells with amplified MCL1 where BETis increase MCL1 protein levels. Furthermore, we identified molecular markers and mechanisms of response to combined BET and MCL1 inhibition in diverse breast cancer cell models. This was achieved with a highly generalizable strategy for the discovery of drug combinations in cancer. In our approach, we integrated high-throughput omics profiling, perturbation biology, network modeling, genomics and functional studies.

Experimental validation in a panel of breast cancer cell lines coupled with genomic analyses in large patient cohorts identified MCL1 copy number as a major predictor for response to combined inhibition of MCL1 and BETis. MCL1 amplification is a well characterized prognostic factor in breast cancer, suggesting that MCL1 targeted therapy may be a viable therapeutic strategy either alone or in combination with HER2 targeted therapies (Campbell et al., 2018, and Berger et al., 2018). Here we showed that MCL1i was effective even with a low level MCL1 amplification and that breast cancer cells are further sensitized to MCL1 inhibition when combined with BETis. From a translational perspective, this is particularly important because, MCL1 high level amplifications are observed in 15% of breast cancer patients, and the frequency of low-level gains in MCL1 is 57%. Therefore, in total, 72% of breast cancer patients are within the potential candidate cohort for MCL1 targeting as a single agent or in combinations. MCL1 amplification is particularly enriched in the basal subtype (32%), the aggressive subtype for which no targeted therapy option exists. Although we observed a clear distinction in responses to MCL1/BET co-targeting between

MCL1 copy number/mRNA high versus low cells, the degree of response was not dependent on the precise level of MCL1 amplification. Both high- and low-level chromosomal gains of MCL1 were equally predictive of responses.

As MCL1 function is also affected by upstream signaling (e.g., GSK3-β) and high turnover rates of the protein (Ding et al., 2007, and Okamoto et al., 2014), we also studied the signaling mechanisms that may contribute to the accumulation of MCL1. The perturbation-biology-based mechanistic studies and differential mRNA/protein expression analysis identified a multi-step mechanism that couples BET inhibition to apoptosis. In resistant cells, BET inhibition upregulates a cell adhesion, motility and fatty acid synthesis metabolic program, which includes the upstream transcription factor SREBF1 (Yokoyama et al., 1993) and key enzymes such as Stearoyl-CoA desaturase (SCD), which converts saturated fatty acids (SFA) into monounsaturated fatty acids and modulates membrane fluidity (Paton et al., 2009, and Ntambi, 1999). SCD has been suggested as a key modulator of breast cancer cell motility and survival as well as EGFR activation in lung cancer (Angelucci et al., 2018, Nashed et al, 2012). Molecular and imaging-based analysis of SCD perturbations demonstrates that SCD activates HER2/EGFR signaling through the remodeling of membrane composition and increased cell membrane fluidity. In turn, we show that HER2/EGFR activation triggers activities of multiple signaling pathways to stabilize MCL1 protein. However, no individual signaling pathway activity is sufficient to drive MCL1 accumulation. For MCL1 upregulation, a combined effect from multiple upstream pathways (AKT/PI3K, RAF/MEK, MAPK14, PKC) converging on GSK3 is necessary as demonstrated by pathway inactivation and reversal of adaptive responses with cocktails of up to four drugs. When SCD and BETis are applied in combination, SCD inhibition reverses the impact of JQ1 on both HER2/EGFR activation and MCL1 levels. Correlative analyses within TCGA breast cancer data suggest that the observed mechanisms involving BET, fatty acid synthesis and RTK signaling are also represented in large cohorts of breast cancer patients, suggesting that the observed drug responses can be extrapolated to clinical settings. Our integrated analyses suggested concerted roles for MCL1 copy number driven gene/protein expression and BETi induced signaling plasticity. Together they maintain high levels of MCL1 to evade apoptosis and confer resistance to BET inhibition. In summary, we demonstrated that an interplay between cellular plasticity in response to BET inhibition and copy-number alterations in MCL1 creates a vulnerability to combinations of BET and MCL1 inhibitors. The complementarity and interplay between hard-coded genetic structure and drug induced plasticity may provide a solution to the long-standing conundrum on the relative dominance of genomics versus signaling activity in driving resistance to targeted agents (Yaffe, 2019).

Consistent with previous reports (Hölscher et al., 2018, and Korkut et al., 2015), Target Score analysis identified cell cycle arrest signature as a key mechanism of action for BET inhibition. In sensitive lines such as SKOV3, apoptosis accompanies cell cycle arrest, whereas in resistant lines an anti-apoptotic program drives evasion of cell death through MCL1 upregulation. In those cells that do not die after prolonged cell cycle arrest, a BETi induced transcriptional program drives resistance. Interestingly, in resistant cells, increased cell motility accompanies apoptotic evasion. A compelling speculation is that when under stress, resistant cells not only escape apoptosis but also display a tendency to depart from the cellular locations mediating stress potentially reflecting processes inherited through phylogeny.

Other preclinical studies have demonstrated the role of lipid metabolism and cell state plasticity in conferring resistance to therapy. For example, high-mesenchymal cell states are resistant to diverse therapies which stems from their dependence on lipid peroxidase pathways, and as a result converging on the actionable GPX4 enzyme (Yang et al., 2014). The compensatory and alternating roles of SCD and FADS2 enzymes in regulating fatty acid desaturation for cancer cell

survival is further evidence for the interplay between cellular plasticity and lipid metabolism (Vriens et al., 2019). Here, for the first time, we linked epigenetic targeting to cellular and signaling plasticity and their consequential drug escape, which can be overcome with the combination of BET and MCL1 inhibition.

Advancing preclinical discoveries to clinical strategies requires a thorough understanding of the molecular markers, mechanisms of drug action and evidence for generalizability. Genomic profiling has already led to major clinical success in subtype specific treatments such as for HER2-amplified breast cancers (Mendes et al., 2015), BRCA-mutated ovarian and breast cancers (Farmer et al., 2005) or BRAF-mutated melanomas (Bollag et al., 2010). Despite this conceptual revolution and advances in sequencing technologies, durable responses to genetically matched targeted therapies in eligible patient cohorts are limited. As of 2019, only 15% of cancer patients are eligible for a genomics-informed therapy and only 8% of patients benefit from genomics-informed therapy with objective responses (Marquart et al., 2018). The relatively low success rate can be attributed to intra and inter-tumor heterogeneity, limited genomic profiling techniques, genotype-therapy matching criteria, and access to effective drugs. This has led to a strong argument that drug response is not only a function of hard-coded genomic aberrations but also signaling pathway activity, cellular states and plasticity. This argument implies that clinical decision making needs to be supported with diverse molecular profiling methods including proteomics and RNA expression. Yet, robust molecular proteomic and cellular profiling methods that can diversify decision making in precision medicine and improve patient benefit are still lacking. Combined with clinical studies involving analysis of temporal biopsies from patients under therapy, we argue that this computational/experimental study is a prototype for future clinical applications, which will induce durable responses based on combination therapy decisions that are dynamically informed by multi-omic profiles of tumors evolving under cancer therapy.

Materials and Methods

Experimental Methods

Cell lines and cell culture

HCC1954, HCC1937, HCC1419, HCC70, BT20, BT474, SKOV3, SKBr3, MDA-MB-468 and MCF-7 cell lines were obtained from MD Anderson Cancer Center Cell Line Repository and were thawed two weeks before experiments. There were less than 10 passages between thawing of the cells and the experiments described in this study. In general, mycoplasma testing is performed approximately every 3 months on all cell lines used in the laboratory. MCF-7 were maintained in DMEM supplemented with 10% FBS plus antibiotic/antimycotic solution (100U/ml streptomycin and 100U/ml penicillin) (all from Invitrogen). BT20 were maintained in EMEM (Eagle's Minimum Essential Medium) supplemented with 10% FBS. HCC1954, HCC1937, HCC1419, HCC70, SKOV3, SKBR3 and BT474 were maintained in RPMI 1640 supplemented with 10% FBS. All cells were cultured at 37°C in a humidified atmosphere containing 5% CO_2.

Kinase inhibitors and antibodies

The kinase inhibitors used in this study were purchased from Sellekchem (JQ1 and the inhibitors of EGFR, AKT, PKC, MAPK, P38), ChemiEtek (MCL1 inhibitor-S63845) and MedChemExpress (JQ1 and SCD-inhibitor-A939572). Specific antibodies against MCL1, BCL2, BCL-XL, BRD4, cleaved PARP, p-AKT(T308), p-AKT (S473), p-PKC, p-P38, p-MEK1/2, p-GSK3, and p-HER2 (T1248)/p-EGFR (Tyr1173) were purchased from Cell Signaling (Cell Signaling Technology, MA). Antibody against β-actin and CellBrite Cytoplasmic Membrane Dyes were from Sigma-Aldrich (St. Louis, MO), Biotium, respectively. Anti-hERBB2/Her2 Alex488 antibody was purchased from R&D systems Biotechne.

RPPA (Reverse Phase Protein Array)
The treatment cells were washed 3 times with cold PBS and then suspended in RIPA buffer supplemented with proteinase inhibitor and phosphatase inhibitor (Pierce, Rockford, IL, USA). The cell suspension was vortexed for 15 seconds, placed on end-over-end rotator for 30 min at 4°C and centrifuged at 14,000 x g for 15 min at 4°C. The lysates were prepared to provide 1-1.5mg/ml of total protein lysate. RPPA analysis samples were prepared by adding SDS Sample Buffer, β-mercaptoethanol and RPPA Working Solution to obtain a final concentration of 0.5mg/ml. Samples were heated for 8 min at 100°C, centrifuged 2 min at 14,000 x g and stored at -80°C. The RPPA was performed at the facility core (MD Anderson Cancer Center).

Immunofluorescence imaging experiments
SKOV3 and HCC1954 cells were seeded in coverslips overnight and treated with either vehicle or kinase inhibitors for 48 hours. The cells were fixed with cross-linking method. Cells were switched to fresh growth media with 4% paraformaldehyde for 5 minutes. After 2 times washing with PBS, the cells were incubated in 4% paraformaldehyde (in PBS) for 15 minutes. The fixed cells were rinsed with PBS to remove any fixation agent. Cells were then blocked with odyssey PBS for 1 hour at room temperature and incubated with the anti-hERBB2/Her2 Alex488 antibody (1:200, R&D systems biotechne) and Cellbrite orange (1:200, Biotium) overnight at 4 ◦C. After washing with PBS, coverslips were mounted on slides using Prolong gold antifade mountant with DAPI (ThermoFisher Scientific, P36935). Immunofluorescence images were acquired with a confocal microscope (Olympus).

Immunoblotting
HCC1954, BT474 and SKOV3 cells were lysed in RIPA buffer (50mM Tris-HCl pH7.4, 150mM NaCl, 1mM EDTA, 1% D.O.C. (Na), 0,1% SDS, 1% Triton X-100) containing protease inhibitors (Pierce, Rockford, IL USA). Protein concentrations were determined using BCA protein assay kit (Pierce, Rockford, IL). An equal amount of proteins was loaded into SDS-PAGE gels and transferred to PVDF membranes (Millipore, MA). Membranes were blocked for 2 hours with 5% non-fat milk in PBST (0.1% Tween-20 in PBS), and incubated overnight with specific primary antibody. After incubation of 2 h with horseradish peroxidase–conjugated secondary antibody, the proteins were detected by Clarity Western ECL substrate (Bio-Rad).

Cell proliferation assays.
Cell proliferation was measured by the PrestoBlue Cell Viability Assay kit (A13261, Life Technologies) according to the manufacturer's instructions. $2\sim4\times10^3$ cells were seeded into 96-well plates and cultured overnight. After treating with either vehicle or kinase inhibitors for 72 hours, cells were collected and evaluated with a SYNERGY H1 microplate reader with Gen5 software (BioTek). In the viability assays, points and bars represent the mean of triplicates ± SEM.

Flow cytometric analysis of cell cycle and apoptosis
2.5×10^5 of cells (HCC1954, BT474 and SKOV3) were seeded in 6-cm plates. Following treating with vehicle or kinase inhibitors for 72 h, cells were harvested, fixed in 1% (W/V) paraformaldehyde in PBS, washed and rehydrated in PBS. DNA was stained according to the instruction of the APO-BRDU™ Kit, by treating the cells with DNA labeling solution, FITC labeled anti-BrdU antibody solution and PI/RNase staining buffer. Flow cytometry was analyzed using BD LSR II flow cytometer and FACSDIV 8.1 software (BD Biosciences) at MDACC flow cytometry core facility.

Migration assays
The effect of drugs on cells' migratory behavior was analyzed by the scratch wound assay. 4×10^5 HCC1954 and SKOV3 cells were seeded in 35 mm dishes. The next day, cells were treated with

vehicle or kinase inhibitors for 72 h. The cells were scratched using a sterile 200-µl micropipette tip to form a straight wound. The cells were washed twice with PBS and cultured for an additional 24 h. The wound closure was measured under an EVOS FL Auto microscope (Life technologies). Images of 3 random fields were acquired at the time point of 0, 6, 12 and 24 h after wounding. The distances traveled by the cells were measured from control and experimental samples and were calculated and compared with time 0.

Membrane fluidity

Membrane fluidity was measured using the Membrane Fluidity Kit (Abcam ab189819). After a lipophilic pyrene probe incorporation into the membrane, the monomeric pyrene probe undergoes excimer formation dramatically shifting the emission spectrum of the pyrene probe to a longer red wavelength. The ratio of excimer (emission at 470 nm) to monomer (emission at 400 nm) fluorescence represents a quantitative change of the membrane fluidity. Cells were seeded in 96 well plate, treated with JQ1, SCD1 inhibitor and JQ1 plus SCD1 inhibitor for 72 hours. The cells were labeled with labeling solution (15 µM of pyrenedecanoic acid (PDA), 0.08% F-127, in Perfusion Buffer) in the dark for 20 min rocking at 25 ◦C, washed 2x with Perfusion Buffer, added culture medium and measured for fluorescence at two wavelengths (excitation at 360 nm, emission at 400 nm and 470 nm). Samples are profiled as biological triplicates.

mRNA Sequencing

Cells (HCC1954, SKOV3 and BT474) were collected after treating with 1 µM of JQ1 for 24 hours all in biological duplicates. Total RNA was isolated and purified using RNeasy Plus Mini Kit (Qiagen). After quantification with Qubit 2.0 (Life Technologies), the samples passed through quality control steps for sample integrity and purity with Agilent 2100 and Agarose Gel Electrophoresis. After the sample QC, the cDNA library is constructed using the NEBNext Ultra II RNA Library Prep Kit (NEB) as follows: mRNA is enriched using oligo(dT) beads. The mRNA is then fragmented via sonication in fragmentation buffer, followed by cDNA synthesis using random hexamers and reverse transcriptase. After first-strand synthesis, a custom second strand synthesis buffer and enzyme mix is added to generate the second strand by nick translation. The final cDNA library is ready after a round of DNA purification, end-repair, A-tailing, ligation of sequencing adapters, size selection and PCR enrichment. For library QC, library concentration was quantified using a Qubit 2.0 fluorometer (Life Technologies) and then diluted to 1 ng/µl before checking insert size on an Agilent 2100. Libraries were then quantified to greater accuracy by quantitative PCR (Q-PCR) prior to sequencing. RNA libraries were sequenced with 20M paired-end 150bp reads on the Illumina NovaSeq 6000 platform (Novogene Inc.). Raw data was subjected to a round of QC to remove low quality reads. The resulting mRNA sequence count data was normalized to enable cross sample analyses.

Computational Methods

Target Score algorithm

The target score algorithm works in multi-steps involving the construction of a reference network, target score calculation, statistical assessment of scores, and the determination and visualization of response pathways. A more technical description and evaluation of the method is presented in Wang et al. - in preparation.

Input Data and data quality. The molecular response data collected before and after therapy is used as the input in the analysis pipeline. The BETi RPPA response is generated at the MDACC functional proteomics core facility. The functional proteomics core validates each antibody by analysis of western blots to observe each readout as a single or dominant band on a blot and ensure the Pearson correlation coefficient between RPPA and western blot readouts are greater

than 0.7. The dynamic range and specificity are routinely determined using peptides, phosphopeptides, growth factors, Inhibitors, RNAi, cells with wide levels of expression including 330 cell lines under multiple conditions on a single array. The intra and inter-slide reproducibility of RPPA reads are routinely monitored. In this study, BETi responses from cell lines are interrogated using 218 antibodies at time points of 24 and 48 hours after drug treatment in cells cultured as 2D monolayers and 3D matrigel cultures. However, the method can analyze data from both patient biopsy samples and cell lines.

Reference network construction. Network models are constructed using the signaling data stored in Pathway Commons (PC) database and manual curation/correction by experts. PC integrates detailed human pathway data from multiple public resources such as Reactome, NCI PID, PhosphoSitePlus, Panther Pathways, and HumanCyc (Cerami et al., 2011). Automated pathway extraction is achieved using the SignedPC algorithm embedded in the BioPAX/PaxTools pathway analysis language and software suite (Demir et al., 2013, Demir et al., 2010, and Babur et al., In Press). In order to delineate the pathway interactions captured by the RPPA data, we identified 4 different relation types: phosphorylation, dephosphorylation, expression upregulation, and expression downregulation. The first two relations can be used to explain phospho-protein changes, and the last two can be used to explain total protein or gene expression changes. Using the BioPAX-pattern framework, we define a set of patterns to detect such relations and identify the signaling interactions between the phosphoproteomic entities. The resulting interaction set defines the reference network.

The Target score and target detection. A Target Score (TS) that quantifies the adaptive pathway responses to a perturbation as a sum of the response from each individual protein and its pathway neighborhood is calculated for each entity. The calculation combines the cell type specific drug response data with signaling network information extracted from signaling databases. High target score identifies proteins involved in adaptive response (e.g., upregulation of receptor tyrosine kinase expression by MEK inhibitor via a feedback loop[4]) and low Target Score corresponds to the immediate impact of the drug (e.g., inhibition of ERK phosphorylation by MEK inhibitor). The mathematical formulation of Target Score is

Equation 1

$$TS_i^d = fs_i\left(\frac{\Delta x_i^d}{\sigma_{\Delta x_i}} + \sum_j 2^{-p}\frac{\Delta x_j^d}{\sigma_{\Delta x_j}}W_{ij}\right)$$

$$\Delta x_i = \log\left(\frac{x_i^p}{x_i^u}\right)$$

$$fs_i = \begin{cases} 1, & if\ oncogene \\ 0, & if\ dual\ or\ unknown \\ -1, & if\ tumor\ suppressor \end{cases}$$

$$W_{ij} = \begin{cases} 1, & if\ phosphorylation\ or\ upregulation \\ -1, & if\ dephosphorylation\ or\ downregulation \end{cases}$$

,where fs_i represents the functional score (see below) of the node of interest, Δx_i is the proteomic response, log normalized with respect to the unperturbed (or pretreatment) level. The σ is the standard deviation of Δx_i over all samples in the study and all drug doses. Division of Δx by σ normalizes a readout with respect to the dynamic range of the corresponding antibody. Node j is a node in the pathway neighborhood of the node i, with readout Δx_j and standard deviation. p_{ij} is the pathway distance between nodes i and j. W_{ij} represents the signaling interaction between

nodes i and j extracted algorithmically from databases. The cumulative Target Score over multiple doses can be calculated as the area under the curve of TS versus drug doses.

A functional score (*fs*) is assigned to each of the proteomic entities measured in the MDACC RPPA and DFCI/MSKCC Zeptosens proteomics platforms (Tibes et al., 2006, and Jing et al., In Press). We used manual curation, resources such as Phosphosite database and TUSON tumor suppressor/oncogene resource (Davoli et al., 2013) results. We assigned (+1) for total levels or activating phosphorylation of oncoproteins and inhibitory phosphorylation of tumor suppressors. Similarly, a functional score of (-1) is assigned to total levels or activating phosphorylation of tumor suppressors and inhibitory phosphorylation of oncoproteins.

The statistical assessment detects and eliminates the Target Scores that are likely driven solely by the network structure with no significant impact from the cell type-specific data. For this purpose, the probability of observing a given Target Score is calculated over a null distribution of Target Score values generated with randomized drug response data and the fixed network structure. A random sampling of proteomic responses (randomized antibody label mixing) at each drug dose generates randomized data sets over all antibody readouts. The Target Score is calculated for 1000 independent random datasets using equation 1, and the null TS distribution is constructed. Next, the FDR-adjusted P value is calculated for the TS value from actual data. For increased statistical power, the p-values across biologically similar or highly overlapping conditions (e.g., similar BETis) that lead to similar Target Scores are merged using the Stouffer's method with the formula (Stouffer et al., 1949).

Equation 2

$$Z = \frac{\sum_{i=1}^{k} Z_k}{\sqrt{k}}$$

Z scores are obtained through p-value-to-Z conversion and k is the total number of conditions merged. Resulting Z-value is back converted to P-values and FDR-adjusted using the Benjamini-Hochberg method.

Determine response pathways. The resistance and response (drug activity) pathways are detected by reanalysis of the Target Score and the underlying network models. Proteins which are connected within the first neighborhood of each other in the underlying network and have highest Target Scores (20 top entities) represent the potential adaptive response pathway(s) and those with low Target Scores represent the potential response/drug activity pathway. The pathway relations are extracted from the reference network model and visualized using the Cytoscape software (Shannon et al., 2003).

Go-Term enrichment

We downloaded GO-term gene associations from http://geneontology.org/gene-associations/goa_human.gaf.gz, and tested enrichment of the terms in differentially expressed 126 genes using Fisher's exact test. We used Benjamini-Hochberg method to select the significance threshold to get a result set with 0.1 FDR.

Differential analysis of omics response

The proteomic response was quantified by normalizing the median normalized proteomic readouts from drug treated samples with respect to the matched untreated samples. The proteomic differential response (Figure 5) is quantified as the $S_{t,i,} = \sum_d[S_t[(\Delta X^{t,d}_{HCC1954,i} - \Delta X^{t,d}_{SKOV3,i}) + (\Delta X^{t,d}_{BT474,i} - \Delta X^{t,d}_{SKOV3,i})]$, where Δx is the phosphoproteomic response for entity i, t is the time point (24 or 48h), and d represents BETi (JQ1, IBET151, IBET726, or IBET762). The statistical significance is quantified using a t-test followed by a Bonferroni multiple hypothesis

correction with the null hypothesis Ho: $\mu(X^{t,d}_{HCC1954,i}) = \mu(X^{t,d}_{SKOV3,i})$. The transcriptomic response was quantified by normalizing the mRNA counts from drug treated samples with respect to the matched untreated samples. The significant mRNA fold changes upon drug treatment were detected as FDR adjusted Q-values < 0.05 with DESeq method. To eliminate noise from rare transcripts, we included the mRNA species with an- abundance over a minimal threshold (minimum count > 200), in at least one condition (i.e., before or after treatment in at least one cell line). The differential responses are visualized as a heatmap that demonstrates fold differences of mRNA species that change in opposite directions in resistant vs. sensitive lines.

Quantification of cell viability drug response

The drug response is quantified as area under the curve, quantified as treating the dose response area as a sum of the trapezoids generated by the responses to consecutive drug doses. The maximum drug dose is quantified as $A_{max} = 1-V_{max}$, where A is the effect at maximum dose and V is the observed viability at maximum dose. The drug synergy is quantified as the Bliss score with the formula; $CI= E_{AB}/(E_A-E_A(1-E_B))$, where E is the effect to drugs A, B and AB (combination of drugs A and B).

Acknowledgement

This work is supported with grants from MD Anderson Cancer Center Support Grant P30 CA016672 (the Bioinformatics Shared Resource), OCRF Collaborative Research Award, U.S. National Cancer Institute grant number 5U24CA210950.

References

1. Holohan, C., Van Schaeybroeck, S., Longley, DB., and Johnston, PG. (2013). Cancer drug resistance: an evolving paradigm. Nat. Rev. Cancer 13, 714-726.
2. Kim, TK., Herbst, RS., and Chen, L. (2018). Defining and Understanding Adaptive Resistance in Cancer Immunotherapy. Trends Immuno. 8, 624-631.
3. Taylor, KN., and Schlaepfer, DD. (2018). Adaptive Resistance to Chemotherapy, A Multi-FAK-torial Linkage. Mol. Cancer Ther. 17, 719-723.
4. Bennet, RL., and Licht, JD. (2018). Targeting Epigenetics in Cancer. Annu. Rev. Pharmacol. Toxicol. 58, 187-207.
5. Loven, J., Hoke, HA., Lin, CY., Lau, A., Orlando, DA., Vakoc, CR., Brander, JE., Lee, TI., and Young, RA. (2013). Selective inhibition of tumor oncogenes by disruption of super-enhancers. Cell 153, 320-334.
6. Alqahtani, A., Choucair, K., Ashraf, M., Hammouda, D.M., Alloghbi, A., Khan, T., Senzer, N., and Nemuaitis, J. (2019). Bromodomain and extra-terminal motif inhibitors: a review of preclinical and clinical advances in cancer therapy. Future Sci OA. 5(3): FSO372.
7. Risom, T., Langer, EM., Chapman, MP., Rantala, J., Fields, AJ., Boniface, C., Alvarez, MJ., Kendsersky, ND., Pelz, CR., Johnson-Camacho, K., Dobrolecki, LE. et al. (2018). Differentiation-state plasticity is a targetable resistance mechanism in basal-like breast cancer. Nat. Commun. 9, 3815.
8. Doroshow, DB., Eder, JP., and LoRusso, PM. (2017). BETis: a novel epigenetic approach. Ann. Oncol. 8, 1776-1787
9. Rathert, P., Roth, M., Neumann, T., Muerdter, F., Roe, JS., Muhar, M., Deswa,l S., Cerny-Reiterer, S., Peter, B., Jude, J. et al. (2015). Transcriptional plasticity promotes primary and acquired resistance to BET inhibition. Nature 525, 543-547.
10. Sun, C., Yin, J., Fang, Y., Chen, J., Jeong, KJ., Chen, X., Vellano, CP., Ju, Z., Zhao, W., Zhang, D. et al. (2018). BRD4 Inhibition Is Synthetic Lethal with PARP Inhibitors through the Induction of Homologous Recombination Deficiency. Cancer Cell 33, 401-416.

11. Andrieu, G., Belkina, AC., and Denis, GV. (2016). Clinical trials for BETis run ahead of the science. Drug Discov. Today Technol. 19, 45-50.
12. Muranen, T., Selfors, LM., Worster, DT., Iwanicki, MP., Song, L., Morales, FC., Gao, S., Mills, GB., and Brugge JS. (2012). Inhibition of PI3K/mTOR leads to adaptive resistance in matrix-attached cancer cells. Cancer Cell 21, 227-239.
13. Duncan, JS., Whittle, MC., Nakamura, K., Abell, AN., Midland, AA., Zawistowski, JS., Johnson, NL., Granger, DA., Jordan, NV., Darr, DB. et al. (2012). Dynamic reprogramming of the kinome in response to targeted MEK inhibition in triple-negative breast cancer. Cell 149, 307-321.
14. Ding, C., Chan, DW., Liu, W., Liu, M., Li, D., Song, L., Li, C., Jin, J., Malovannaya, A., Jung, SY. et al. (2013). Proteome-wide profiling of activated transcription factors with a concatenated tandem array of transcription factor response elements. Proc. Natl. Acad. Sci. USA 110, 6771-6776.
15. Arumugam, T., Ramachandran, V., Fournier, KF., Wang, H., Marquis, L., Abbruzzese, JL., Gallick, GE., Logsdon, CD., McConkey, DJ., and Choi, W. (2009). Epithelial to mesenchymal transition contributes to drug resistance in pancreatic cancer. Cancer Res. 69, 5820-5828.
16. Dang, CV., Reddy, EP., Shokat, KM., and Soucek, L. (2017). Drugging the 'undruggable' cancer targets. Nat. Rev. Cancer 17, 502-508.
17. Fey, SJ., and Wrzesinski, K. (2012). Determination of drug toxicity using 3D spheroids constructed from an immortal human hepatocyte cell line. Toxicol. Sci. 127, 403-411.
18. The Cancer Genome Atlas Network (2012). Comprehensive molecular portraits of human breast tumours. Nature 490, 61-70.
19. Meric-Bernstam, F., Frampton, GM., Ferrer-Lozano, J., Yelensky, R., Pérez-Fidalgo, JA., Wang, Y., Palmer, GA., Ross, JS., Miller, VA., Su ,X. et al. (2014). Concordance of genomic alterations between primary and recurrent breast cancer. Mol. Cancer Ther. 13, 1382-1389.
20. Xu, Y., and Vakoc, CR. (2017). Targeting Cancer Cells with BET Bromodomain Inhibitors. Cold Spring Harb Perspect Med. 7, pii: a026674.
21. Stouffer, S.A., Suchman, EA., DeVinney, LC., Star, SA., and Williams, RM. Jr. (1949). The American Soldier, Vol.1: Adjustment during Army Life. Princeton University Press, Princeton.
22. Zhang, S., Zhao, Y., Heaster, TM., Fischer, MA., Stengel, KR., Zhou, X., Ramsey, H., Zhou, MM., Savona, MR., Skala, MC. et al. (2019). BETis reduce cell size and induce reversible cell cycle arrest in AML. J. Cell Biochem 120, 7309-7322.
23. Sahni, JM., Gayle, SS., Bonk, KL., Vite, LC., Yori, JL., Webb, B., Ramos, EK., Seachrist, DD., Landis, MD., Chang, JC. et al. (2016). Bromodomain and Extraterminal Protein Inhibition Blocks Growth of Triple-negative Breast Cancers through the Suppression of Aurora Kinases. J. Biol. Chem. 291, 23756-23768.
24. Barretina, J., Caponigro, G., Stransky, N., Venkatesan, K., Margolin, AA., Kim, S., Wilson, CJ., Lehár, J., Kryukov, GV., Sonkin, D. et al. (2012). The Cancer Cell Line Encyclopedia enables predictive modelling of anticancer drug sensitivity. Nature 483, 603-607.
25. Kotschy, A., Szlavik, Z., Murray, J., Davidson, J., Maragno, AL., Le Toumelin-Braizat, G., Chanrion, M., Kelly, GL., Gong, JN., Moujalled, DM. et al. (2016). The MCL1 inhibitor S63845 is tolerable and effective in diverse cancer models. Nature 538, 477-482
26. Adams, KW., and Cooper, GM. (2007). Rapid turnover of mcl-1 couples translation to cell survival and apoptosis. J. Biol. Chem. 282, 6192-6200.
27. Mojsa, B., Lassot, I., and Desagher, S. (2014). Mcl-1 ubiquitination: unique regulation of an essential survival protein. Cells 3, 418-437.
28. Röhrig, F., and Schulze, A. (2016). The multifaceted roles of fatty acid synthesis in cancer. Nat. Rev. Cancer. 16, 732-749.

29. Stubbs, CD., and Smith, AD. (1984). The modification of mammalian membrane polyunsaturated fatty acid composition in relation to membrane fluidity and function. Biochim. Biophys. Acta. 779, 89-137.
30. Roongta, UV., Pabalan, JG., Wang, X., Ryseck, RP., Fargnoli, J., Henley, BJ., Yang, WP., Zhu, J., Madireddi, MT., Lawrence, RM. et al. (2011). Cancer cell dependence on unsaturated fatty acids implicates stearoyl-CoA desaturase as a target for cancer therapy. Mol. Cancer Res. 1, 1551-1561.
31. Kim, JB., and Spiegelman, BM. (1996). ADD1/SREBP1 promotes adipocyte differentiation and gene expression linked to fatty acid metabolism. Genes Dev. 10, 1096-1107.
32. Ramsey, HE., Fischer, MA., Lee, T., Gorska, AE., Arrate, MP., Fuller, L., Boyd, KL., Strickland, SA., Sensintaffar, J., Hogdal, LJ. et al. (2018). A Novel MCL1 Inhibitor Combined with Venetoclax Rescues Venetoclax-Resistant Acute Myelogenous Leukemia. Cancer Discov. 8, 1566-1581.
33. Campbell, KJ., Dhayade, S., Ferrari, N., Sims, AH., Johnson, E., Mason, SM., Dickson, A., Ryan, KM., Kalna, G., Edwards, J. et al. (2018). MCL-1 is a prognostic indicator and drug target in breast cancer. Cell Death Dis. 9, 19.
34. Berger, AC., Korkut, A., Kanchi, RS., Hegde, AM., Lenoir, W., Liu, W., Liu, Y., Fan, H., Shen, H., Ravikumar, V. et al. (2018). A Comprehensive Pan-Cancer Molecular Study of Gynecologic and Breast Cancers. Cancer Cell. 33, 690-705.
35. Ding, Q., He, X., Hsu, JM., Xia, W., Chen, CT., Li, LY., Lee, DF., Liu, JC., Zhong, Q., Wang, X. et al. (2007). Degradation of Mcl-1 by beta-TrCP mediates glycogen synthase kinase 3-induced tumor suppression and chemosensitization. Mol. Cell Ciol. 27, 4006-4017.
36. Okamoto, T., Coultas, L., Metcalf, D., van Delft, MF., Glaser, SP., Takiguchi, M., Strasser, A., Bouillet, P., Adams, JM., and Huang, DC. (2014). Enhanced stability of Mcl1, a prosurvival Bcl2 relative, blunts stress-induced apoptosis, causes male sterility, and promotes tumorigenesis. Proc. Natl. Acad. Sci. USA 111, 261-266.
37. Yokoyama, C., Wang, X., Briggs, MR., Admon, A., Wu, J., Hua, X., Goldstein, JL., and Brown, MS. (1993). SREBP-1, a basic-helix-loop-helix-leucine zipper protein that controls transcription of the low density lipoprotein receptor gene. Cell 75:187-197.
38. Paton, CM., and Ntambi, JM. (2009). Biochemical and physiological function of stearoyl-CoA desaturase. Am. J. Physiol. Endocrinol. Metab. 297, E28-37.
39. Ntambi, JM. (1999). Regulation of stearoyl-CoA desaturase by polyunsaturated fatty acids and cholesterol. J. Lipid Res. 40, 1549-1558.
40. Angelucci, C., D'Alessio, A., Iacopino, F., Proietti, G., Di Leone, A., Masetti, R., and Sica, G. (2018). Pivotal role of human stearoyl-CoA desaturases (SCD1 and 5) in breast cancer progression: oleic acid-based effect of SCD1 on cell migration and a novel pro-cell survival role for SCD5. Oncotarget 9, 24364-24380.
41. Nashed, M, Chisholm, JW, Igal, RA, (2012) Stearoyl-CoA desaturase activity modulates the activation of epidermal growth factor receptor in human lung cancer cells. Exp. Biol. Med., 237, 1007-1017
42. Yaffe, MB. (2019). Why geneticists stole cancer research even though cancer is primarily a signaling disease. Sci. Signal 12, pii: eaaw3483.
43. Hölscher, AS., Schulz, WA., Pinkerneil, M., Niegisch, G., and Hoffmann, MJ. (2018). Combined inhibition of BET proteins and class I HDACs synergistically induces apoptosis in urothelial carcinoma cell lines. Clin Epigenetics 10, 1.
44. Korkut, A., Wang, W., Demir, E., Aksoy, BA., Jing, X., Molinelli, EJ., Babur, Ö., Bemis, DL., Onur Sumer, S, Solit, DB. et al. (2015). Perturbation biology nominates upstream-downstream drug combinations in RAF inhibitor resistant melanoma cells. Elife 4, e04640.

45. Yang, WS., SriRamaratnam, R., Welsch, ME., Shimada, K., Skouta, R., Viswanathan, VS., Cheah, JH., Clemons, PA., Shamji, AF., Clish, CB. et al. (2014). Regulation of ferroptotic cancer cell death by GPX4. Cell 156, 317-331.
46. Iwamoto, H., Abe, M., Yang, Y., Cui, D., Seki, T., Nakamura, M., Hosaka, K., Lim, S., Wu, J., He, X. et al. (2018). Cancer Lipid Metabolism Confers Antiangiogenic Drug Resistance. Cell Metab. 28, 104-117.
47. Vriens, K., Christen, S., Parik, S., Broekaert, D., Yoshinaga, K., Talebi, A., Dehairs, J., Escalona-Noguero, C., Schmieder, R., Cornfield, T. et al. (2019). Evidence for an alternative fatty acid desaturation pathway increasing cancer plasticity. Nature 566, 403-406.
48. Neel, DS., and Bivona, TG. (2017). Resistance is futile: overcoming resistance to targeted therapies in lung adenocarcinoma. NPJ Precis Oncol. 1, pii:3.
49. Sabnis, AJ., and Bivona, TG. (2019). Principles of Resistance to Targeted Cancer Therapy: Lessons from Basic and Translational Cancer Biology. Trends Mol. Med. 25, 185-197.
50. Groenendijk, FH., and Bernards, R. (2014). Drug resistance to targeted therapies: déjà vu all over again. Mol. Oncol. 8,1067-83.
51. Dumbrava, EI., and Meric-Bernstam, F. (2018). Personalized cancer therapy-leveraging a knowledge base for clinical decision-making. Cold Spring Harb. Mol. Case Stud. 4, pii: a001578.
52. Kurnit, KC., Bailey, AM., Zeng, J., Johnson, AM., Shufean, MA., Brusco, L., Litzenburger, BC., Sánchez, NS., Khotskaya, YB., Holla, V. et al. (2017). "Personalized Cancer Therapy": A Publicly Available Precision Oncology Resource. Cancer Res. 77, 123-126.
53. Mendes, D., Alves, C., Afonso, N., Cardoso, F., Passos-Coelho, JL., Costa, L., Andrade, S., and Batel-Marques, F. (2015). The benefit of HER2-targeted therapies on overall survival of patients with metastatic HER2-positive breast cancer--a systematic review. Breast Cancer Res. 17, 140.
54. Farmer, H., McCabe, N., Lord, CJ., Tutt, AN., Johnson, DA., Richardson, TB., Santarosa, M., Dillon, KJ., Hickson, I., Knights, C. et al., (2005). Targeting the DNA repair defect in BRCA mutant cells as a therapeutic strategy. Nature 434, 917-921.
55. Bollag, G., Hirth, P., Tsai, J., Zhang, J., Ibrahim, PN., Cho, H., Spevak, W., Zhang, C., Zhang, Y., Habets, G. et al. (2010). Clinical efficacy of a RAF inhibitor needs broad target blockade in BRAF-mutant melanoma. Nature 467, 596-599.
56. Marquart, J., Chen, EY., and Prasad, V. (2018). Estimation of the Percentage of US Patients With Cancer Who Benefit From Genome-Driven Oncology. JAMA Oncol. 4, 1093-1098.
57. Cerami, EG., Gross, BE., Demir, E., Rodchenkov, I., Babur, O., Anwar, N., Schultz, N., Bader, GD., and Sander, C. (2011). Pathway Commons, a web resource for biological pathway data. Nucleic Acids Res. 39, D685-690.
58. Demir, E., Babur, O., Rodchenkov, I., Aksoy, BA., Fukuda, KI., Gross, B., Sümer, OS., Bader, GD., and Sander, C. (2013). Using biological pathway data with paxtools. PLoS Comput. Biol. 9, e1003194.
59. Demir, E., Cary, MP., Paley, S., Fukuda, K., Lemer, C., Vastrik, I., Wu, G., D'Eustachio, P., Schaefer, C., Luciano, J. et al. (2010). The BioPAX community standard for pathway data sharing. Nat. Biotechnol. 28, 935-942.
60. Babur, Ö., Luna, A., Korkut, A., Durupinar, F., Siper, MC., Dogrusoz, U., Aslan, JE., Sander, C., and Demir E. In Press. Causal interactions from proteomic profiles: molecular data meets pathway knowledge. doi: https://doi.org/10.1101/258855
61. Tibes, R., Qiu, Y., Lu, Y., Hennessy, B., Andreeff, M., Mills, GB., and Kornblau, SM. (2006). Reverse phase protein array: validation of a novel proteomic technology and utility

for analysis of primary leukemia specimens and hematopoietic stem cells. Mol. Cancer Ther. 5, 2512-2521.

62. Jing, X., Wang, W., Gauthier, NP., Kaushik, P., Root, A., Stein, RR., Korkut, and A., Sander, C. In Press. Protein profiling in cancer cell lines and tumor tissue using reverse phase protein arrays. doi**:** https://doi.org/10.1101/144535
63. Davoli, T., Xu, AW., Mengwasser, KE., Sack, LM., Yoon, JC., Park, PJ., and Elledge, SJ. (2013). Cumulative haploinsufficiency and triplosensitivity drive aneuploidy patterns and shape the cancer genome. Cell 155, 948-962.
64. Shannon, P., Markiel, A., Ozier, O., Baliga, NS., Wang, JT., Ramage, D., Amin, N., Schwikowski, B., and Ideker, T. (2003). Cytoscape: a software environment for integrated models of biomolecular interaction networks. Genome Res. 13, 2498-2504.
65. Liu, Y., Beyer, A., and Aebersold, R. (2016). On the Dependency of Cellular Protein Levels on mRNA Abundance. Cell 165, 535-550.
66. Gry, M., Rimini, R., Strömberg, S., Asplund, A., Pontén, F., Uhlén, M., and Nilsson, P. (2009). Correlations between RNA and protein expression profiles in 23 human cell lines. BMC Genomics 10, 365.

SUPPLEMENTARY FIGURES

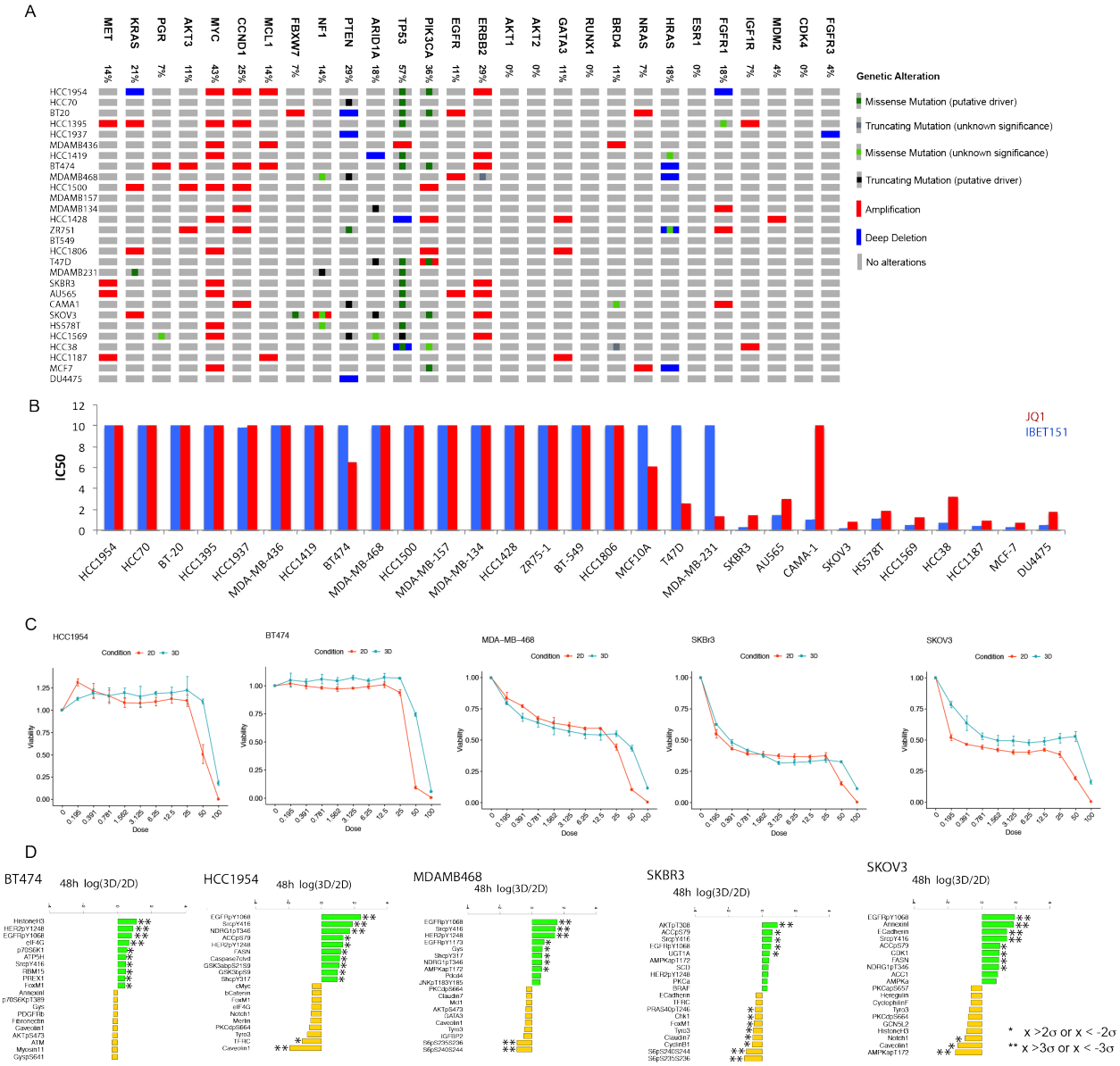

Figure S1. A. Genomic alteration profiles in the breast cancer and SKOV3 cell lines treated with BETis. The order of cell lines reflects BETi sensitivity rank (top: most resistant, bottom: most sensitive). Genes that are frequently altered in breast cancer are included in the analysis. **B.** BETi (JQ1 and IBET151) cell viability response IC50 for cell lines. **C.** Dose response curves of BET inhibition in HCC1954, BT474, MDAMB468, SKBR3, and SKOV3 cultured in 2D and 3D. **D**. Impact of ECM attachment in 3D cultures on proteomic levels in all cell lines. The bar plots display relative values with respect to those in monolayered cultures. Most significant increases are noted in EGFR phosphorylation at Y1068 (up to 2.4 increase in all cell lines except SKOV3), HER2 phosphorylation at Y1248 (log-fold increase of 0.4 in SKBR3 to 1.4 in SKOV3), HistoneH3 levels (1.2 log2-fold increase in BT474) and SRC phosphorylation at Y416 (up to 2 log-fold increase in all cell lines). Most significant reduction induced by ECM attachment were in S6 phosphorylation at S235/236 and S240/244 (~1 log2-fold decrease in SKBR3 and MDAMB468), caveolin (2 log2-fold decrease in HCC1954) and AMPK_pT172 (1.6 log-fold decrease in SKOV3). AKT phosphorylation at T308 was increased in SKBR3; E-cadherin and annexin were increased in

SKOV3 upon ECM attachment. Interestingly, lipid metabolism genes such as FASN and ACC1 (total and phosphorylated state) were higher in 3D cultured HCC1954 and SKOV3 lines

2D

24h 48h

HCC1954

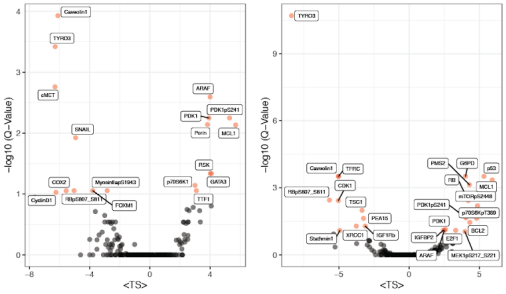

3D

24h 48h

BT474

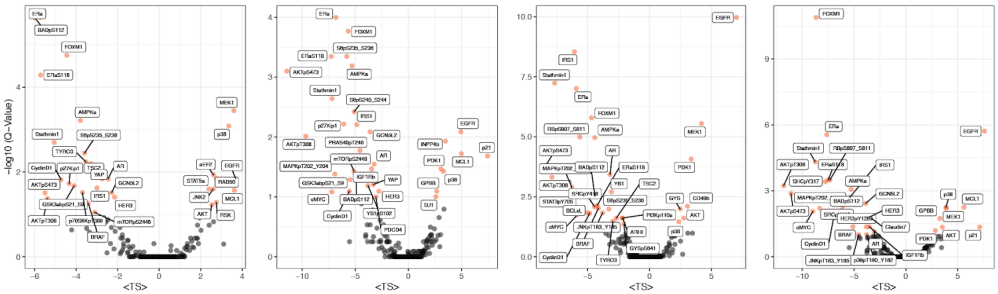

MDAMB468

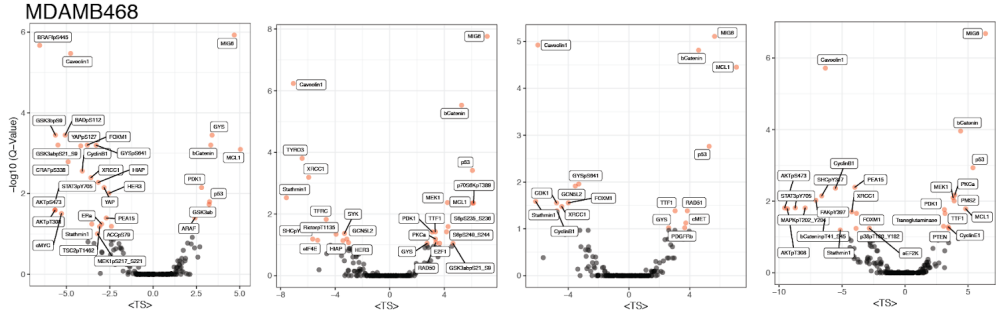

SKBR3

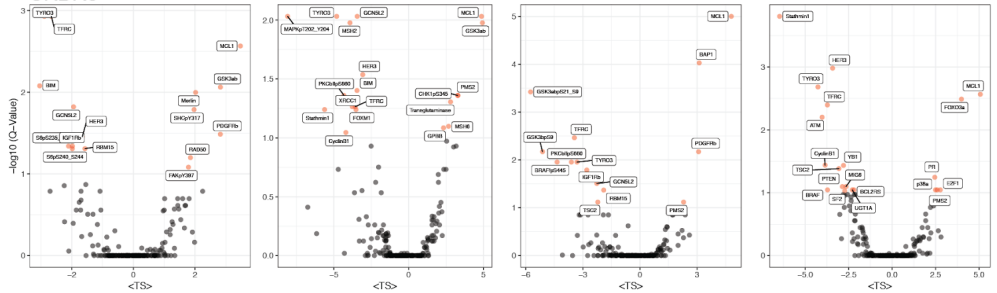

SKOV3

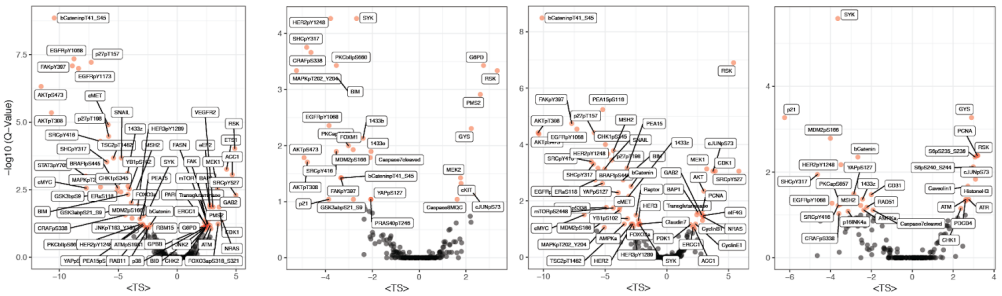

Figure S2. Target Score analysis of HCC1954, SKOV3, BT474, MDAMB468 and SKBR3 lines treated with BETis in 2D and 3D cultures based on RPPA data collected 24 and 48 hours post perturbation.

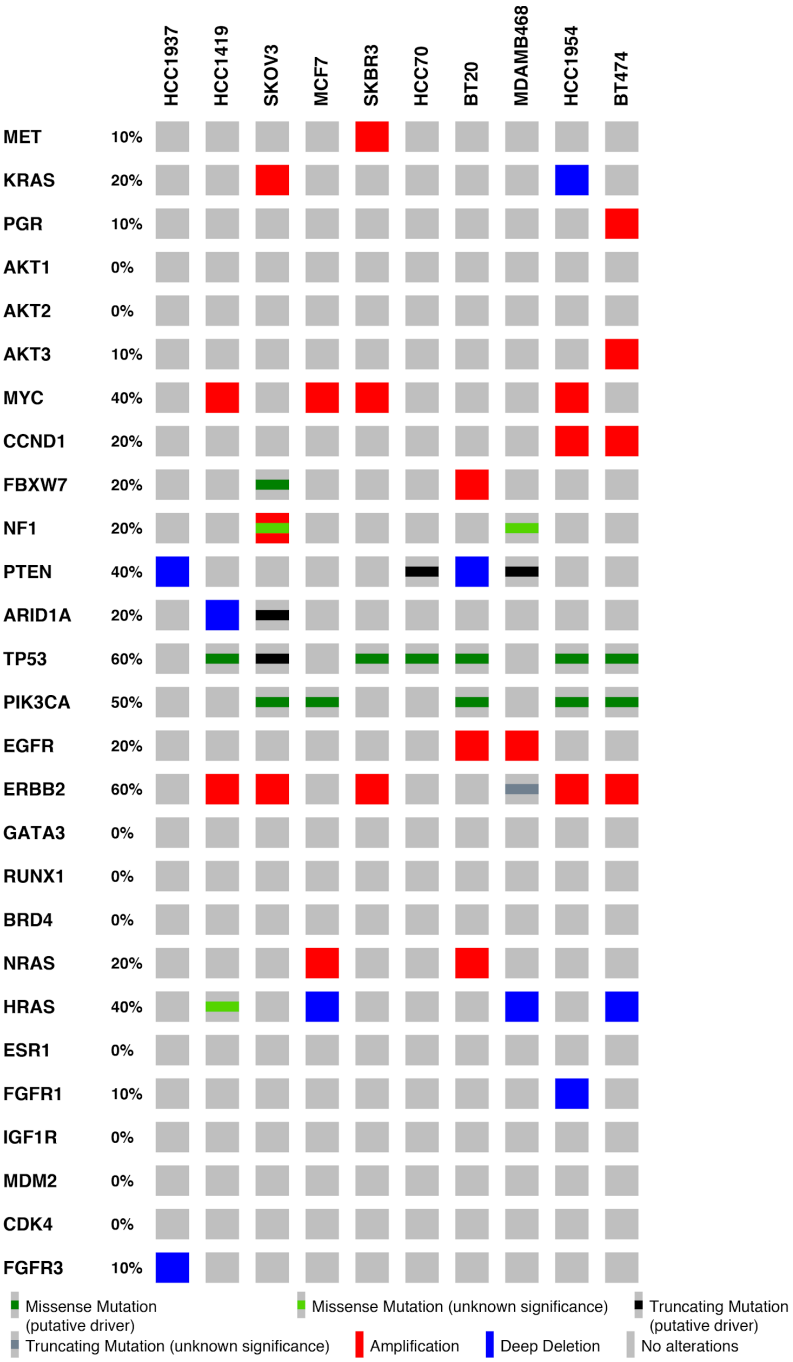

Figure S4. The genomic alterations in the breast and ovarian (SKOV3) cell lines tested with the BET and MCL1 inhibitor combination.

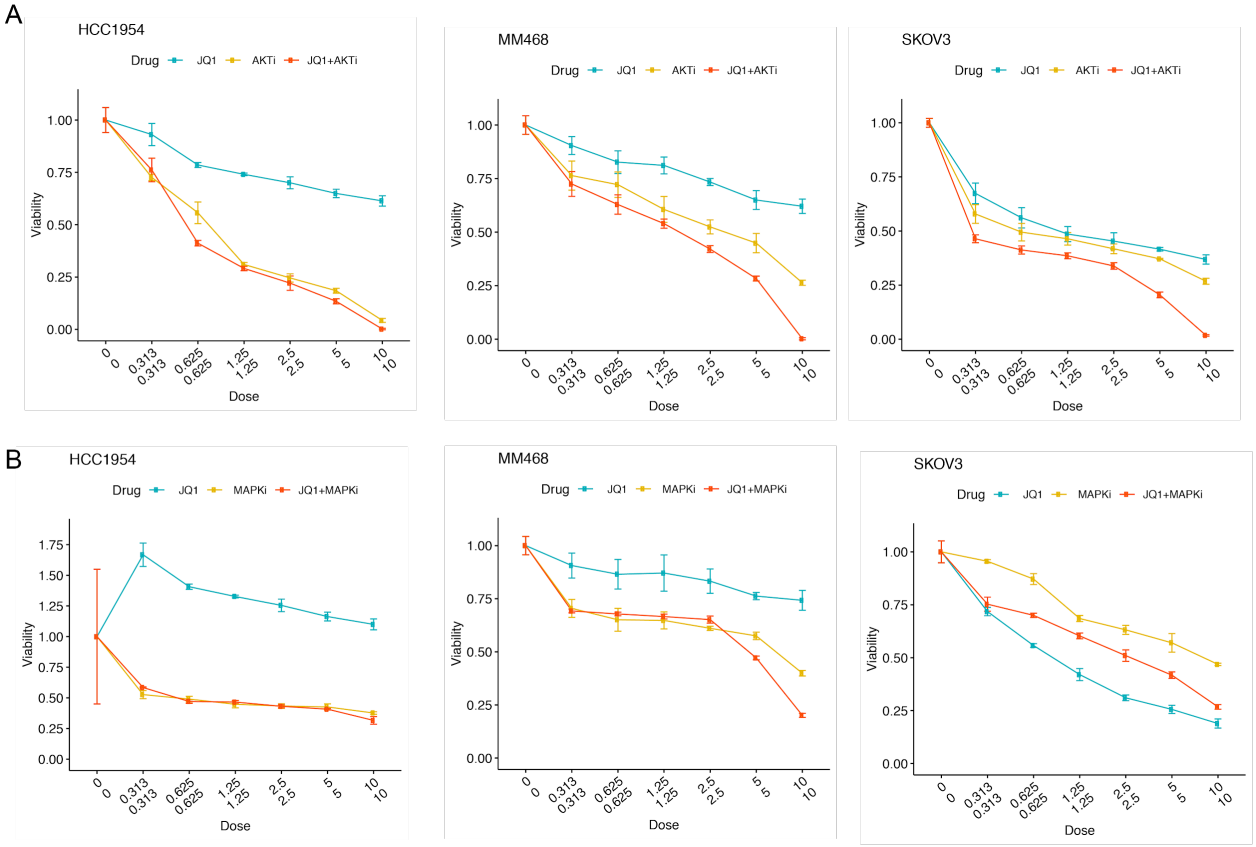

Figure S5. The cell viability response to combination of BET inhibitors with **A**. AKT inhibitor, **B.** MEK1/2 inhibitors (trametinib).